Insight into the Katari-Lago Menor Basin aquifer, Lake Titicaca-Bolivia, inferred from geophysical (TDEM), hydrogeological and geochemical data

Gabriela Patricia Flores Avilés, Marc Descloitres, Céline Duwig, Yvan Rossier, Lorenzo Spadini, Anatoly Legchenko, Álvaro Soruco, Jaime Argollo, Mayra Pérez, Waldo Medinaceli

Insight into the Katari-Lago Menor Basin aquifer, Lake Titicaca-Bolivia, inferred from geophysical (TDEM), hydrogeological and geochemical data

Gabriela Patricia Flores Avilés [1,2 a], Marc Descloitres [1], Céline Duwig [1], Yvan Rossier [1], Lorenzo Spadini [1], Anatoly Legchenko [1], Álvaro Soruco [3], Jaime Argollo[3], Mayra Pérez [3], Waldo Medinaceli [4]

[1] Univ. Grenoble Alpes, CNRS, IRD, Grenoble-INP*, IGE, 38000 Grenoble, France
[2] Ministerio de Educación Estado Plurinacional de Bolivia (Ministry of Education, MINEDU), La Paz, Bolivia
[3] University Mayor of San Andrés (UMSA), La Paz, Bolivia
[4] Ministerio de Medio Ambiente y Agua (Ministry of Environment and Water of Bolivia), La Paz, Bolivia
* Institute of Engineering, Univ. Grenoble Alpes

Abstract

The increasing demand for water and irrigation in the semi-arid Bolivian Altiplano requires a better knowledge of the available resources, particularly groundwater. The aim of this study is to provide a first insight into the hydrogeological structure (0-200 m deep) and groundwater dynamics of the Katari-Lago Menor Basin aquifer located between the Eastern Cordillera and Lake Titicaca, Bolivia. This aquifer is studied using geophysical data (a total of 187 Time Domain Electromagnetic (TDEM) soundings), piezometric data (97 groundwater level measurements) and geochemical data (52 groundwater samples), combined with geological, lithological and topographical information.

The results allowed identifying stratigraphic models consistent with the Quaternary sediments being hydraulically connected and behaving as a single regional basin-aquifer. This basin-aquifer is delimited by the most ancient lake invasions towards the southern, western and northern sides and by the lower limit of rock glaciers towards the eastern side. A large portion of the aquifer presents an unconfined behaviour varying from 50 to 150 meters while the confined portion varies from 100 to 150 meters.

Groundwater flow within the Katari and Lago Menor Basin aquifer is composed of several interconnected groundwater flow systems. The main groundwater flow system starts in the high mountain ranges of the Eastern Cordillera, follows the topographic Piedmont gradient (NE to SW) and discharges in a series of wetlands.

This multidisciplinary approach proved to be an appropriate method to derive a consistent picture of the hydrogeological functioning of the Katari-Lago Menor Basin aquifer.

Keywords: Katari-Lago Menor Basin aquifer, groundwater resources, Time-Domain Electromagnetic soundings

[a] Corresponding author.
E-mail address: gpfloresaviles@gmail.com (GP Flores Avilés)

1. Introduction

Water quality degradation, climate variability and population growth are among the factors that constrain water availability in the semi-arid Bolivian Altiplano (Coudrain et al., 1994; Guérin et al., 2001; Garcia et al., 2010; Archundia et al., 2017a, 2017b; Guédron et al., 2017; Quino et al., 2019; Gómez et al., 2019) and in the central parts of Bolivia (Gonzáles-Amaya et al., 2018a, 2018b), leading to an increasing exploitation of groundwater resources.

In the Katari and Lago Menor Basin (Fig.1), one of the most populated and contaminated basins of the Bolivian Altiplano (BID, 2016; Agramont et al., 2019), melt water from the high peak glaciers of the Eastern Cordillera and groundwater withdrawals, are both important sources of water supply for domestic drinking, industry and irrigation purposes (M.M.A.yA, 2014; Soruco et al., 2015; Kinouchi et al., 2019). Recent research predicted that climate variability and population growth will most likely lead to a water shortage after the mid-2020s (Kinouchi et al., 2019) which could intensify groundwater exploitation in order to meet the growing demand.

To contribute to the sustainable management of groundwater resources within the Katari and Lago Menor Basin, the understanding of the main natural flow processes of the groundwater system at the basin scale is essential for developing numerical groundwater flow models, evaluating recharge, discharge, aquifer storage, and sustainable yield. Previous investigations on the site showed local-scale hydrogeological characterizations based on lithology, groundwater level measurements, hydrochemistry and stable isotopes of deuterium and oxygen 18 (M.M.A.yA, 2016; Quino et al., 2019). However,

63 the lack of geophysical information did not allow the identification of vertical, lateral or
64 spatial variation of the permeable Quaternary geologic media nor the bottom boundaries
65 of the aquifer or aquifers (depth to bedrock).

66 Additionally, former geological studies showed profiles describing general geological
67 formations to a depth of 1 km (Ballivian et al., 1978; GEOBOL & Swedish Geological
68 AB, 1995). This vertical scale is not suitable for the assessment of shallow (0-200 m)
69 groundwater investigations. Indeed, in this depth range, the thickness and lateral extent
70 (geometry), hydraulic properties and hydrostratigraphic units of the aquifer are not
71 known.

72 Moreover, little is known about the potential influence of sewage, waste disposal,
73 farmland and mining activities on groundwater resources of the basin (Barroso, 2010;
74 M.M.A.yA, 2016; Quino et al., 2019; Archundia et al., 2017b). Actually, most of the
75 rural communities in the basin rely mainly on groundwater either from wells, springs or
76 wetlands. However, they lack of adequate disposals of sewage and human waste
77 (M.M.A.yA, 2014). A basin-scale groundwater investigation is necessary for
78 understanding the main physical, chemical and biological processes.

79 The understanding of the main natural flow processes of the groundwater system
80 requires the delimitation of the domain, the determination of the boundaries and initial
81 conditions, and the physical characteristics of the porous media. A combination of tools
82 is needed to adequately characterize the aquifers in this region. Previous research across
83 the world, including South America, have shown that the application of
84 multidisciplinary studies can contribute to the understanding of the functioning of
85 complex hydrogeological systems (Guerin et al., 2001; Ramos et al., 2014; Mira et al.,
86 2015; Gómez et al., 2016; Gómez et al., 2019; Gonzales Amaya et al., 2018a, 2018b;
87 Maldonado et al., 2018; Viguier et al., 2018).

88 The aim of this study is to provide a first characterization of the aquifer at the scale of
89 the Katari and Lago Menor Basin. To achieve, this objective, we conducted a
90 multidisciplinary study (geology, geophysics, geochemistry, and groundwater level
91 measurements). The specific objectives were to determine: i) the spatial limits of the
92 aquifer, ii) the vertical and lateral variation of the Quaternary geologic media, iii) the
93 bottom boundaries of the aquifer (depth to the top of the Tertiary/Devonian bedrock),

and to characterize iv) the groundwater flow dynamics at the scale of the Katari-Lago Menor Basin.

Finally, we propose a 3D conceptual model of the aquifer structure and its functioning as a basis for assessing the current knowledge of groundwater resources, possible development of numerical models and therefore development of future groundwater management strategies in the Bolivian Lake Titicaca region.

2. Background information on the study area

The study site is located within the Katari and Lago Menor Basin, in the semi-arid region of the Bolivian Northern Altiplano. The Katari and Lago Menor Basin is a sedimentary basin with an approximate area of $6350\ km^2$ and it is bounded by the high mountains of the Eastern Cordillera, the southeast of Lake Titicaca (Lago Menor or Lake Huiñamarca) and the outcropping rock formations towards the Tiwanaku, Comanche and Colquencha Cities (Fig.1).

Previous studies have documented that Lake Titicaca comprises two, nearly separated basins connected by the strait of Tiquina:(i) the Lago Menor (also called in some studies Huiñamarca) Basin (Fig.1) averaging 1428 km² and 9 m depth (up to 40 m depth) and (ii) the Lago Grande Basin averaging 7131 km² and 125 m depth (up to 284 m depth) (Cross et al., 2001; Fritz et al., 2006; Fritz et al., 2007).

2.1 Geology

The Katari and Lago Menor Basin consists of erosional landforms in Tertiary and Paleozoic sedimentary rock formations that are filled up with Pleistocene to Holocene sediments (Fig. 1). These landforms were influenced by Quaternary glaciations of different ages and extensions. These Quaternary glaciations are related to the Andes Cordillera uplift and large-scale climatic patterns (Argollo and Iriondo, 2008; Araos et al., 2017; Emmer t al., 2019). Indeed, wet and cold conditions during regional glacial advance (glacial cycles) and warm and dry conditions during regional glacial retreat (interglacial cycles) (Fritz et al., 2007), are the main climatic patterns that favoured the formation of glacial and lacustrine landforms between the high mountains of the Bolivian Eastern Cordillera and Lake Titicaca region (Argollo and Mourguiart, 2000;

123 Cross et al., 2001; Abbott et al., 2003; Fritz et al., 2006; Fritz et al., 2007; Zech et al.,
124 2007; Bush et al., 2010; Plackzec et al., 2011; Quesada et al., 2015).

125 Therefore, the deposits that fill up the Katari and Lago Menor basin result from glacial
126 erosion of the Paleozoic (Silurian/ Devonian) sedimentary sequence from the high
127 mountain ranges, and lake expansions and evaporation processes in the lower sectors
128 (Ballivian, 1978; Lavenu, 1992; Argollo and Mourguiart, 1995; Heine, 2004; Zech et
129 al., 2007; Argollo and Iriondo, 2008). Lavenu (1992) classified these deposits as: i)
130 glacial and interglacial deposits in the high peaks and on the piedmont, ii) torrential
131 fluviatile deposits on the piedmont and high plain, and iii) lacustrine evaporite deposits
132 in the plateau. Additionally, the occurrence of alluvial fan deposits in the study area is
133 controlled by topography. They are formed close to steep sided mountains or hills
134 (waved glacial deposits) flanked by areas of low relief (Fig.1).

135 In this paper, we propose to describe our results considering two major
136 geomorphological domains: the "Piedmont subsystem" and the "Lacustrine plain".

137 The "Piedmont subsystem" starts from the outcropping Silurian formations (in the high
138 mountain ranges of the upper eastern area) and reaches the outcropping Devonian
139 formations (i.e. Dvv and Dbl) to the southwest (towards Pucarani, Laja and Viacha
140 Cities) (Fig.1). The Piedmont subsystem is subdivided into the upper and lower
141 Piedmont areas (Fig.1). The upper Piedmont area corresponds to a significant
142 accumulation of glacial and fluvioglacial outwash deposits (Ballivian, 1978; Lavenu,
143 1992; Argollo and Mourguiart, 2000; Argollo and Iriondo, 2008), whereas the lower
144 Piedmont area is characterized by fluvial-alluvial and/or fluvioglacial outwash deposits
145 sometimes overlying ancient lacustrine deposits. Additionally, the occurrence of two
146 alluvial fans formed at the mouths of the Tuni and Condoriri rivers in the NW and the
147 Sorechata and Pampasi rivers in the SE, are denominated as major and minor alluvial
148 fans, respectively (Fig.1).

149 The "Lacustrine plain" is bounded by those Devonian formations (i.e. Dvv and Dbl) and
150 the Tertiary formations (i.e. Tkk, Tcn and Ttc) outcropping between the Taraco, Collana
151 and Colquencha Cities (Fig.1). The Lacustrine plain is characterized by the presence of
152 lacustrine deposits that are related to the ancient lake invasions. According to Lavenu
153 (1992), the present Lake Titicaca overlays deposits from Paleo-lake Ballivian "Ulloma

154 Formation, Qull" (Fig.1) which hosts vast clay resources (Zeballos et al., 2017), while
155 deposits from the most ancient Paleo-lakes Mataro and Cabana underlying the Ulloma
156 Formation are series of fluviatile detrital deposits (Table 1).

157 Generally, the thickness of these Quaternary deposits, their spatial continuity, and the
158 depth to bedrock, are poorly known. Preceding geological studies showed profiles with
159 a vertical scale (1 km) not suited for hydrogeological assessments (Ballivian et al.,
160 1978; GEOBOL & Swedish Geological AB, 1995). The Quaternary glaciation history
161 indicates that the permeable Quaternary geologic sediments could be associated with:
162 Early-Pleistocene glacial deposits, Late-Pleistocene fluvioglacial outwash deposits, or
163 Late-Pleistocene lacustrine deposits (Table 1).

164 Furthermore, the Tertiary/Devonian/Silurian sedimentary sequence is dominated by
165 shales and sandstones (Lamb and Hoke, 1997; Salvaderry-Aranguren et al., 2008;
166 Murray et al., 2010; Zeballos et al., 2017). These sedimentary units are rich in ore and
167 clay minerals and are extracted for the mining and ceramic industries (Sugaki and
168 Kitakaze, 1988; Salvaderry-Aranguren et al., 2008; Zeballos et al., 2017). However,
169 there is no evidence that they are significant aquifers with exploitable groundwater. In
170 this study, these Tertiary and Paelozoic sedimentary formations are assumed to be the
171 impervious bottom of the Quaternary geologic media containing water.

172 Considering the recognized glacial-interglacial cycles and lake expansions between the
173 Bolivian Eastern Cordillera and the Bolivian Northern Altiplano, the lithostratigraphy
174 and geological structure that make up the Katari and Lago Menor Basin, are shown in
175 Figure 1 and listed in Table 1 (from younger to older) (Ballivian, 1978; Lavenu, 1992;
176 GEOBOL & Swedish Geological AB, 1995; Suárez-Soruco and Díaz-Martínez, 1996;
177 Argollo and Mourguiart, 2000; Heine, 2004; Argollo and Iriondo 2008; Fritz et al.,
178 2004; Salvaderry et al., 2008; Murray et al., 2010; Sánchez-Saldías and Fariña, 2014;
179 Zeballos et al., 2016 ; Zeballos et al., 2017).

180 ***2.2 Climate***

181 The climate in the Katari and Lago Menor region could be described as South American
182 Summer Monsoon reported in several studies for the Northern Altiplano (Condom et al.,
183 2004; Placzek et al., 2011; Canedo et al., 2016). It presents a cold and semi-arid climate
184 with a marked 'Rainy season' (October to March) and 'Dry season' (April to

September). The annual precipitation and evapotranspiration also varies across the basin and depends mainly on the local topography.

In the high peak glaciated areas (Huayna Potosí, Condoriri glaciers) of the Eastern Cordillera (Fig.1), the mean annual precipitation varies from 577 to 750 $mm\ year^{-1}$ (Rabatel et al., 2006; Veettil et al., 2018; Kinouchi et al., 2019) while the sublimation and evaporation in these glaciated areas accounts for 222 $mm\ year^{-1}$ (Kinouchi et al., 2013). Additionally, on the piedmont, daily long-term variations (2009-2018) of precipitation recorded at El Alto airport station (Fig.1) showed that the mean annual precipitation reaches 614 $mm\ year^{-1}$ and the mean annual potential evapotranspiration 1158 $mm\ year^{-1}$. Finally, in the lower sectors, long-term variations of precipitation reported by Geerts et al. (2009), at the Huarina station (Fig.1), showed that the mean annual precipitation reaches up to 513 $mm\ year^{-1}$, whereas the estimated actual crop evapotranspiration for quinoa cultivation would vary around for 350 to 500 $mm\ year^{-1}$.

2.3 Hydrogeological setting of the study area

Previous local-scale research has investigated and monitored groundwater resources primarily in the two largest cities of the Katari and Lago Menor Basin (El Alto and Viacha, Fig.1) (M.M.A.yA, 2016). M.M.A.yA (2014) delimited the Purapurani zone (370 Km^2) (Fig.2) according to the lithology and general stratigraphy of the Quaternary deposits: fluvioglacial and alluvial deposits surrounded by glacial deposits to the north, and the Paleozoic rocks towards the west and south.

The lithological information of several boreholes drilled in the Purapurani zone to a depth of 60 to 110 meters (GEOSIRH, 2017) indicated that the Quaternary geologic media is saturated. However, there are no studies that reported the total thickness of these deposits (depth to bedrock) or their spatial continuity (hydraulic continuity).

Field data from two pumping tests performed by M.M.A.yA established that fluvioglacial materials in the Purapurani zone behave as potential permeable layers with a hydraulic conductivity ranging from $1.3 \times 10^{-6}\ to\ 2.0 \times 10^{-4}\ m/s$. Moreover, long-term groundwater level monitoring data (50 observation wells) have shown that groundwater flow direction, towards NE to SW in this zone, is consistent with flow

from the high surface elevations to the low elevations. Close to the east boundary, groundwater flow diverts in the SE direction, towards the valleys of the City of La Paz (M.M.A.yA, 2016).

Barroso (2010) conducted a detailed hydrogeological assessment in the location of El Alto Sanitary landfill (Fig.2), towards the NE of the Purapurani zone. This author concluded that the landfill had been placed over clayey glacial-till materials of granite blocks, quartzite, quartzes and intermingled sand, with horizontal hydraulic conductivities ranging from $1.2 \times 10^{-8}\ to\ 3.3 \times 10^{-7}\ m/s$.

The wetland ecosystems are other significant features that could be part of the groundwater system. Several investigations around the world have shown that in arid and semi-arid regions, wetland ecosystems can be associated with discharge areas of regional gravity-driven groundwater flow systems (Foster et al., 2006; Tóth et al., 1999). In the study area, the wetlands located in the lower sectors of the Piedmont subsystem (Fig. 1) are associated with groundwater discharges controlled by the topography and geology (i.e. large alluvial fans). Another type of wetlands, formed over impermeable subsurface layers (i.e. clay deposits), are encountered in the Lacustrine plain. According to Melly et al. (2017) these type of wetlands, overlying hard or impermeable subsurface layers are called "perched wetlands".

Finally, the presence of active or inactive rock glaciers located in the upper part of the basin, in the Tuni Condoriri valley and near the Huayna Potosí glacier (Rangecroft et al., 2014), could also be linked to the regional groundwater system as a recharge source for the aquifer. Rangecroft et al. (2016) demonstrated that these rock glaciers would become relict forms, by the end of the century, due to future climate warming. Relict rock glaciers are complex hydrogeological systems with high storage capacity (Winkler et al., 2016; Harrington et al., 2018) that might act as relevant groundwater storages (Pauritsch et al., 2017; Jones et al., 2019).

3. Materials and Methods

In this study, the general methodology that facilitated the interpretation and compilation of hydrogeological results are deduced from the application of a multidisciplinary approach (geology, geophysics, geochemistry, and groundwater level measurements).

This approach was proved to be useful in other groundwater systems in South America (Guerin et al., 2001; Ramos Ramos, 2014; Mira et al., 2015; Gómez et al., 2016; Gómez et al., 2019; Gonzales Amaya et al., 2018a, 2018b; Maldonado et al., 2018; Viguier et al., 2018).

For instance, several studies can be cited in the northern Chile such as the multidisciplinary study conducted by Viguier et al. (2018) in the hyperarid Atacama Desert, the multi-method assessment performed by Oyarzún et al. (2014) in the semi-arid Limarí River basin, and the groundwater recharge assessment carried out in the arid Salar del Huasco basin (Uribe et al., 2015). Additionally, in Argentina, Mira et al. (2015) integrated geological and geophysical data to build a geological subsurface model for the Corrientes province aquifer. Maldonado et al. (2015) combined hydrogeochemical and groundwater level data to assess the deep aquifers from the Pampean plain (Maldonado et al., 2015). Furthermore, in Brazil, Fernandes et al. (2016) used physical and structural geology data to develop a preliminary conceptual model of groundwater flow for the Serra Geral basalt aquifer.

In Bolivia, local groundwater investigations mainly relate the application of geophysical techniques. For example, Guérin et al. (2001) used geophysical surveys and groundwater electrical conductivity measurements to identify saline groundwater in the semi-arid Bolivian Altiplano. Gómez et al. (2019) performed electromagnetic soundings and electrical resistivity tomography to investigate the thickness of an alluvial aquifer and to delineate the relief of the bedrock. Gonzáles Amaya et al. (2018a) used hydrogeophysics to refine hydrogeological conceptual models. Additionally, these authors (Gonzales Amaya et al., 2018b) used transient electromagnetic soundings for mapping saline water zones in the semiarid Punata alluvial fan, in the Central part of Bolivia. Following those approaches, we used a combination of geophysical, groundwater levels and geochemical measurements.

3.1 Time Domain Electromagnetic (TDEM) soundings

3.1.1 TDEM principle

Time Domain Electromagnetic (TDEM) is a geophysical sounding method based on the investigation of the electrical resistivity of rocks. Resistivity is a well-known parameter in hydrogeophysics. For our study, electrical resistivity is a well adapted parameter

because our objective is to discriminate permeable formations from more clayey formations, possibly identify conductive brackish groundwater close to the lake (if any) or any lateral variations of groundwater electrical conductivity. Previous studies have demonstrated the usefulness of TDEM for groundwater investigations in arid and semi-arid areas, as highlighted by Descloitres et al. (2013) in the semiarid Lake Chad Basin (Niger), Viguier et al. (2018) in the hyperarid Atacama Desert (Northern Chile), or by Guérin et al. (2001) and Gonzales Amaya et al. (2018) in the semiarid Altiplano (Bolivia).

Basically TDEM uses a large transmitter (Tx) square loop (typically 50x50m² or 100x100m²) and a receiver loop (Rx) both laid out on the surface. Rx can be either a small coil at the centre of Tx (central loop system), or be the same cable as Tx (coincident loop system, as used in our study). A direct current is injected in Tx creating a primary static magnetic field that diffuses into the ground. Once the primary magnetic field is established, the current is abruptly turned-off creating a decreasing flux with time. Due to the induction principle, eddy currents are then created in the soil immediately below Tx cable. As the time elapse, and because the primary magnetic field no longer exists, the eddy current are decreasing with time and further current loops are created deeper and expand laterally in the sub-surface, as smoke rings. Each eddy current loop creates a secondary magnetic field (with the same polarity that the primary magnetic field) also decreasing with time, creating an induced current in Rx loop. The result (the decreasing voltage with time) is then analysed to derive the basic information given by TDEM: the sounding curve, i.e the variation of apparent resistivity with time. Field data are then fitted to simulated data curves, using a layered resistivity model of the ground by means of an automatic adjustment (inversion) of a starting 1-D model with a minimum of layers (usually 3). If the RMS calculated after the inversion remains high (i.e. above 2-3 %) one or two additional layers are introduced to smooth the model and decrease the RMS. The final results are interpreted as a 1-D (layered) model of the resistivity with depth, which can be related to the geology and related aquifers. Further information can be found in the comprehensive review of TDEM for groundwater exploration published by Fitterman and Stewart (1986).

306 *3.1.2 TDEM survey strategy and interpretation*

307 The locations of the TDEM profiles were chosen in order to investigate the different
308 outcropping formations (Tertiary/Devonian substratum) and the different Quaternary
309 deposits (alluvial fan, fluvioglacial, glacial, paleo-lacustrine and fluvio-lacustrine
310 deposits). The locations of these profiles are presented in Figure 2.

311 Profile 1 is 44 km long (75 soundings, Table 2), and has a NE-SW direction. It stretched
312 from the Eastern Cordillera to the Piedmont subsystem and the Lacustrine plain. This
313 profile investigated also Devonian and Tertiary formations perpendicular to their main
314 structural direction. It crosses Quaternary glacial and fluvioglacial deposits, alluvial fan
315 deposits, and paleo-lacustrine deposits.

316 Profile 2 is 33 km long (32 soundings, Table 2), and has a SE-NW direction. It is
317 perpendicular to profile 1 is used to explore Quaternary fluvioglacial, alluvial fan and
318 paleo-lacustrine deposits.

319 Profile 3 of 26 km long (16 soundings, Table 2), located between the lake (Cohana Bay)
320 and the lower Piedmont area, investigates paleo-lacustrine and alluvial fan deposits. It
321 also explores a zone where we hypothesised the presence of a subterranean channel for
322 groundwater flow interconnecting the Piedmont subsystem and Lacustrine plain.

323 Profile 4 was 24 km long (30 soundings, Table 2), has a NE-SW direction. This profile
324 was designed to perpendicularly cross Devonian and Tertiary formations as well as
325 Quaternary fluvio-lacustrine deposits close to Lake Titicaca.

326 Profiles 5, 6 and 7 (6 km, 3 km and 6km long, respectively) have a NW-SE direction
327 and included 7 to 10 soundings each (Table 2). They are located on the shores of Lake
328 Titicaca (Cohana and Puerto Perez Bays) to understand the geometry of Quaternary
329 paleo-lacustrine deposits, that interact directly with Lago Menor.

330 Additional TDEM soundings were performed near boreholes (Fig.2). All in all, TDEM
331 soundings are located close to 30 boreholes from the geodatabase of
332 MMAyA/VRHR/PDCK (M.M.A.yA, 2014) with available lithological logs.

333 Along the profiles, the initial sampling interval was a spacing of 500 m. This distance
334 was considered to be the minimum length required to describe relevant aquifer

heterogeneity. As no major heterogeneity was discovered within the first 10 km of the profile, the distance between the soundings was then increased to 1.5 km separation. A total of 187 TDEM soundings (Table 2) were performed with the TEM-FAST 48 equipment (AEMR technology, The Netherlands). The soundings were performed using a coincident loop configuration, a transmitter/receiver (Tx/Rx) loop of 100 x 100 m² and when urban sites were surveyed, using a 25 x 25 m² coincident receiver loops. Measurements were performed using the maximum possible Tx current (2.1 A). At each location, a set of 200 to 260 individual sounding curves have been recorded and stacked to reduce the electromagnetic noise. An acquisition time was adjusted from few micro-seconds to 400 or even 4000 µs according to the level of noise and subsurface TDEM response. An automatic filtering option has been chosen (including 50 Hz removal). Ambient electromagnetic noise was also recorded daily to provide the necessary information to remove noisy points from the sounding curve. 1-D inversion was performed with TEM-RES software, developed by AEMR technology.

For inversion, several considerations were taken into account. We used 1-D (layered) models to fit the data. The 1-D hypothesis is considered as reasonable in the context of a sedimentary aquifer at the scale of one TDEM sounding (lateral investigation limited to few tens of meters laterally away from the loop of the cable). In a second step, for several TDEM soundings close to boreholes, we tested inversions using: a) three or four resistivity model layers and b) a smooth multilayer resistivity models with 10 to 20 layers. Both, the 3-4 layers and smooth multilayer models, gave acceptable RMS values not greater than 1 to 2 %. We chose to use the simplest resistivity models to easier link geological formations to a unique range of resistivity. Eventually, we chose to conduct a 1-D inversion for each sounding, and not to use a Laterally Constrain Inversion –LCI- procedure (Auken et al, 2005). In our case, even if LCI could be considered in some parts of the survey with a first layer that characterizes a unique geological pattern along long sections (as in the alluvial fans for example), the resistivity of second and third deeper layers greatly vary laterally especially where paleo-valleys or buried Tertiary formations are present. In those areas, no lateral correlations between layers are possible since some models have low resistive layers in the deep section and others have high resistive layers and are close together (few hundreds of meters). In such complicated geology, a LCI procedure would have required a smaller distance between sounding points. For future large surveys, for example for airborne TDEM survey that allows a

shorter distance between sounding points, LCI could be considered, taking advantage of our ground results to adapt the convenient lateral sampling interval between two TDEM soundings.

3.2 Piezometric and geochemical measurements

3.2.1 Groundwater level measurements

The field measurements of water levels were undertaken for a subset of wells/boreholes and groundwater sources in the vicinity of the study area. A total of 97 groundwater sources were validated in the field during August of 2017: 55 deep wells, 32 dug wells, 8 springs and 2 wetlands (Fig.1). Measurements corresponding to water level depths were converted to hydraulic head using sea level as the reference datum. Hydraulic head elevations were used to assess groundwater flow direction and horizontal hydraulic gradients in the study area. The vertical reference, altitude above sea level (m a.s.l), are based on the SRTM-GL1-30 m (Shuttle Radar Topography Mission 1 Arc-Second Global, approximately 30 m resolution, N.A.S.A, 2000) digital elevation model (DEM). The accuracy of this DEM over the Altiplano was tested by Satgé et al. (2016). These authors state that the SRTM-GL1-30 m DEM has a more precise elevation and relative height-pixel accuracy than SRTM-v4 and GDEM-v2, based on STD and RMSE values and bias analysis.

3.2.2 Geochemical sampling and analysis

Groundwater samples were collected from 52 deep wells, 20 to 110 m b.g.l (meters below ground level), mostly by electrical pumps (Fig.1). The sampling strategy was defined in accordance with the TDEM survey, considering the spatial and vertical distribution of the main permeable Quaternary formations. These wells were selected to characterize the geochemical facies of the groundwater and to ascertain the regional groundwater circulation patterns in the basin.

Major ion concentrations (Ca^{2+}, Mg^{2+}, Na^{+}, K^{+}, HCO_3^{-}, Cl^{-}, SO_4^{2-}, NO_3^{-}) were quantified, at the IGE (Institut des Géosciences de l'Environnement) Laboratory, using the Metrohm 732/733 ion chromatograph modular system, precision ±0.1 mg/L, and calibrated with standard solutions Roth (5 to 40 mg/L range). Blanks consisted of ultrapure, (Milli-Q) water. Total alkalinity was measured in the field by titration

(HACH digital titrator method) and recalculated as bicarbonate. A piper diagram, performed with DIAGRAMMES (Simler, 2014), was used to point out the typical groundwater facies of the Katari-Lago Menor aquifer.

4. Results

4.1 Hydraulic head contour map and electrical conductivity variations

Figure 3 displays hydraulic head contours and general flowpaths from the groundwater system. From this figure, five flow systems can be distinguished where recharge mainly comes from the upper Piedmont and from effective infiltration from precipitation.

In the first flow system groundwater moves to the SW and flows into Lake Titicaca (Puerto Pérez Bays) in the northwest (e.g. flowpath 1). In the second flow system groundwater moves into the Lacustrine plain through breaks or channels between the bedrock outcrops and is illustrated by flowpaths 2, 4 and 6. The outlet of this second flow system is probably Lake Titicaca at the level of Cohana Bay. In the third flow system groundwater moves to the SW discharging in a series of wetlands (e.g. flowpath 3) or uplifts into the surface due to the hydraulic barriers of bedrock outcrops, forming also wetlands (e.g. flowpath 5). In the fourth flow system groundwater moves towards the southeast discharging in springs and seepages in the El Alto-La Paz-Achocalla area (e.g. flowpath 6). And finally, the fifth flow system is illustrated by flowpath 8 where groundwater moves slowly to the NW, mainly due to the low hydraulic head gradient (flat slope) and probably due to limited recharge from the Piedmont subsystem.

Figure 3 also depicts groundwater electrical conductivity measurements (EC in $\mu S/cm$) which vary within both geomorphological domains. Indeed, in the Piedmont subsystem, groundwater electrical conductivity values range between 63 to 416 $\mu S/cm$ towards the NW (blue circles) and between 86 to 433 $\mu S/cm$ towards the SE (green circles). Groundwater samples from the Piedmont subsystem are differentiated in colors because the southern zone appears to be more prone to contamination due to mining concessions and the urbanized city of El Alto. In contrast, in the Lacustrine plain groundwater electrical conductivity values range from 530 to 1700 $\mu S/cm$ (cyan circles).

426 ### *4.2 TDEM interpretation*

427 #### *4.2.1 TDEM comparison with boreholes and outcropping geological formations*

428 In order to be able to correlate TDEM resistivity profiles and geology, we conducted as
429 a first step, an analysis of the TDEM soundings performed near boreholes and over the
430 outcropping Tertiary/Devonian formations (i.e. Tcl, Tkk and Dbl, Table 1) (Fig.2).

431 TDEM soundings were performed between 250 m to 2 km of distance from boreholes
432 (Fig.2) due to the presence of villages/houses. Consequently, the correspondence of
433 thicknesses between TDEM and borehole is sometimes poor due to possible lateral
434 changes.

435 Figure 4 displays field data from five representative TDEM soundings and their
436 locations are shown in Figure 2. The layered resistivity TDEM model is presented as a
437 color log beside the borehole log. Groundwater electrical conductivity measured for the
438 majority of the boreholes varies over a relatively narrow range (i.e. between 80 and 200
439 µS/cm) (Fig.3). Therefore, resistivity variations can generally be attributed to changes
440 in geology, not to groundwater electrical conductivity variations. However care should
441 be taken close to the lake, because groundwater conductivity is sometimes increasing
442 (up to 600-1300 µS/cm) indicating a connection with Lake Titicaca (~1000 µS/cm)
443 (Fig.3) or an influence of the evaporitic nature of the paelo-lacustrine formations (i.e.
444 Qcb-mt formation, Table 1).

445 TDEM sounding S-34 (borehole BH-2, 500 m away, EC~106 µS/cm) investigates a
446 shallow clay layer appearing as a unique resistivity layer of 10 Ω·m. Deeper, TDEM
447 model shows a second layer with resistivity values of 33 Ω·m characteristic of an
448 alternation of sand and gravel with thin clayey layers. Then, TDEM shows a more
449 resistive layer, 426 Ω·m not seen in the borehole.

450 TDEM sounding P1-14 (borehole Ae GAP 175, 2 km away, EC~86 µS/cm) investigates
451 a shallow massive sand and gravel formation as a unique resistivity layer of 129 Ω·m.
452 Deeper, TDEM model shows a second layer with resistivity values of 41 Ω.m
453 characteristic of an alternation of sand and gravel with thin clayey layers. Then, TDEM
454 shows a more conductive layer, 18 Ω·m not seen in the borehole.

TDEM sounding S-PUC-11 (borehole BH-6, 1km away, EC~142 µS/cm) investigates gravel and sand deposits with a limited fraction of clay (~ 5%) appearing as a unique resistivity layer of 233 Ω·m. Deeper, TDEM model shows a third layer with resistivity values of 38 Ω·m attributed to more silty or clayey layer not seen in the borehole log.

TDEM sounding S-63 (borehole P-1, 50 m away, EC~600 µS/cm) investigates a fluvio-lacustrine deposit. The first layer is an alternation of thin sand and clay layers as a unique resistivity layer of 51 Ω·m. Deeper, TDEM model shows a second layer with resistivity values of 30 Ω·m while clay layers are becoming more frequent. Then, TDEM shows a more resistive layer, 93 Ω·m not seen in the borehole log.

TDEM sounding P1-5 (borehole Ae-GAP-166 PI3, 250m away, EC~230 µS/cm; Fig.2), investigates fluvio-glacial deposits with shallow layers of gravels and sands appearing as a unique resistivity layer of 109 Ω·m. Below, clay-silt layers present a resistivity value of 35 Ω·m. Deeper, TDEM model shows a third layer with resistivity values of ~16 Ω·m attributed to more clayey layers not seen in the borehole log.

This comparison analysis illustrates two major facts: first, the geology of the area as described by boreholes exhibits most of the time a complicated interstratified medium. Secondly, it illustrates the lack of TDEM resolution of thin, interstratified medium. This well-known limitation of the method arose in our study: fine intercalations of thin, clayey or loamy layers with thin sandy layers at depth cannot be delineated, as confirmed by Descloitres et al. (2013) for a clayey sand aquifer. Therefore, the stratified resistivity model derived from TDEM must be interpreted as a model representing thick geological units only. The resistivity value of those thick units varies with clay content, the greater the number of clayey layers are, the less the resistivity is. This information is a valuable indication for the hydrogeological potential of the aquifer.

The comparison with boreholes allows us to derive resistivity ranges for the Quaternary deposits (i.e. glacial, fluvioglacial, alluvial and paleo-lacustrine deposits). However, none of the borehole information investigates the substratum (i.e. Tertiary or Devonian sedimentary rocks). To evaluate the resistivity range for this substratum we performed some TDEM soundings directly on the outcropping formations (Fig.2). Figure 5 summarizes resistivity ranges for both Quaternary (boreholes) and Tertiary/Devonian

485 (outcrops) and can be used as a guideline to conduct the entire TDEM profile
486 interpretation.

487 From Figure 5 analysis, in the Lacustrine plain, paleo-lacustrine deposits are either
488 clayey (5-15 Ω·m) or clay sandy-gravel layers with intermediate resistivity range (30-40
489 Ω·m). Within the Piedmont subsystem, the resistivity ranges from intermediate values
490 (30-120 Ω·m) and can reach more resistive range (120-300 Ω·m) for alluvial fans and
491 glacial deposits.

492 The substratum underlying the Quaternary geologic media, both within the Piedmont
493 subsystem and Lacustrine plain, are resistive (up to~300 Ω·m) except for the Kollu
494 Kollu Formation (Tkk ~40 Ω·m) due to the presence of gypsum and for the Cachilaya
495 Formation (Tcl ~150 Ω·m) a claystone formation with layers of tuff.

496 ***4.2.2 TDEM profiles***

497 The lateral variations of resistivity along TDEM profiles are displayed in Figures 6 and
498 7. The descriptions of the results are based on the main geomorphological domains, i.e.
499 the Piedmont subsystem and Lacustrine plain. For each domain, the stratigraphic
500 interpretations are based on the interpretations illustrated in Figure 5.

501 ***4.2.2.1 Piedmont subsystem***

502 *Profile 1*

503 The upper Piedmont area in Profile 1 (Fig.2, Fig.6) shows, from surface to depth, a first
504 layer composed of two parts: one is found above 4260 m a.s.l (between TDEM
505 soundings "S0A" and "S1A") and show resistivity values of ~100 to 170 Ω·m and a
506 thickness of 60 to 150 m. This part is attributed to glacial deposits (geological
507 Formation, "Qg") probably from the Sorata glaciation (Table 1). Then, a second part
508 (below 4260 m a.s.l) between soundings S11A-S10A, shows more resistive values
509 (~300 Ω·m) and a thickness of ~125 m, is also attributed to glacial deposits (flow-tills)
510 from the same formation (Qg-Sorata Fm.). From borehole information nearby this
511 second part is composed of poorly sorted clasts/blocks of quartzite, shales and granites
512 in a clayey matrix.

513 Below this first resistive layer, a second layer between soundings S0A and S10A, shows
514 resistivity values of ~60 to 120 Ω·m and a thickness of 60 to 120 m. This layer may
515 belong to deposits from a non-differentiated interglacial/glacial cycle, possibly the
516 fluvio-glacial (Qfg) Purapurani Formation or the glacial (Qg) Calvario Formation,
517 composed of gravel with silt layers or tills and fluvial gravels (Table 1). The same layer
518 is found between soundings S7A and S-9A, showing resistivity values up to ~80 Ω·m
519 and a thickness of 60 to 150 m.

520 Below the above layers, the pattern of the top of the substratum (underlying Quaternary
521 deposits) is found similar to the actual topography of the closest rocky outcrops, located
522 about 2 km from the profile in a NW direction. This noticeable correspondence is a
523 strong indication of a sharp, bedrock topography at the base of the Quaternary deposits,
524 as seen in the section between soundings S8A and S-PUC-07 (Profile 1, Fig.6). This
525 bedrock topography could be the result of the tectonic deformations associated to the
526 Eastern Cordillera and the Altiplano region (i.e. structural features, Fig.1).

527 In the lower Piedmont area (Fig.2, Fig.6), the section between soundings S-PUC-07 to
528 P56 shows an uppermost layer with resistivity values of ~ 250 to 115 Ω·m and a
529 thickness of 40 to 75 m, revealing the geometry of the minor alluvial fan deposits (Qaa)
530 (Fig.1, Table 1). From borehole information nearby, these deposits consist of gravels,
531 sands and clays.

532 Then, below the alluvial fan deposits, a second layer between soundings P63-P59 and
533 P58-P56, shows resistivity values of ~30 Ω·m and a thickness of 50 to 130 m. These
534 sections display paleo-valley geometries with deposits that may be attributable to the
535 ancient Lakes Cabana and Mataro (Table 1) remaining as a unique non-differentiated
536 formation (Qcb-mt) in this interpretation. From borehole information nearby, it
537 comprises clayey sandy and gravelly sand intercalations.

538 In addition, sections P49-SLJ01 and P34-P25 show a first layer with resistivity values
539 of ~40 to 60 Ω·m and a thickness up to 100 m, which may be attributed to fluvio-
540 lacustrine deposits (Qfl), comprised of gravel and sand materials with clay and silt
541 content (Table 1). A deeper, second layer, found in section P49-S-LJ-01 with resistivity
542 values ~30 to 40 Ω·m and a thickness of 40 to 100 m, may belong to deposits from the

(Qcb-mt), both layered formations indicating fluviatile conditions, with alternation of clay, sand and gravel deposits (Table 1).

The vertical resistivity variations in section P49 –S-LJ-01 (from 60 to 30 Ω·m) rather than being different geological formations (.i.e. Qfl and Qcb-mt) may also be due to change in groundwater electrical conductivity.

Profile 2

From Profile 2 (Figure2, Figure 7), we learn additional information about the lower Piedmont area. From NW to SE, Profile 2 shows the transverse geometry of the major alluvial fan deposit separated by the rocky formation (Tpñ), outcropping 1 km towards the NE (Fig. 1, Table 1), as well as the minor alluvial fan deposit in transition with fluvioglacial deposits (Fig. 1).

Towards the NW, the section between soundings T-13 and S16A shows an upper layer with resistivity values ~270 to 370 Ω·m and a thickness up to 85 m, revealing a thick accumulation of alluvial deposits (Qaa), probably Pre-Sorata gravels (Table 1), that are mainly composed of sandy gravel and medium and fine gravels, as evidenced in borehole BH-6.

The section between soundings P1-22 and P1-21 (Fig. 7) shows a first layer with resistivity values of ~140 Ω·m and a maximum thickness of ~20 m, which is attributed as a thin layer of alluvial deposits (Figure 4).

Towards the SE, section P1-20–P1-14 displays a first layer with resistivity values of ~140 to 240 Ω·m and a thickness of 20 to 50 m, which is attributed to deposits from the minor alluvial fan (Qaa), consisting of gravels, sands and clays. Subsequently, the section between soundings P1-13 and P1-1 depicts a first layer with resistivity values of ~100 Ω·m and a thickness of 30 to 70 m, attributed to fluvioglacial outwash sediments (Qfg) from the upper Purapurani Formation (Table 1), which mainly comprises gravel, sand and silt sediments (borehole Ae-GAP-166, Figure 4).

Then, a deeper second layer with resistivity values of ~30 to 40 Ω·m and a thickness of 20 to 50 m is found along the whole section between soundings P1-18 and P1-1, that is attributed to deposits from the ancients Lake Cabana and Mataro (Qcb-mt) (Table 1) composed of alternating clay, sand and gravel deposits. The Purapurani Formation seen

below the city of El Alto has outcropping lacustrine deposits at its base, with a lithology similar to the La Paz Formation (Tlp) (Table 1).

Profile 3

Profile 3 (Fig.2, Fig.7) also investigates the lower Piedmont area. Between soundings T13 and S-PUC-10 (aligned in a NE-SW direction), we can investigate the longitudinal section of the major alluvial fan (Fig. 1). Underlying this section, from soundings S-PUC-12 to S-PUC-10, we can follow a sequence that could be attributed to deposits from the ancient's lake invasions.

The major alluvial fan (Qaa) shows a layer with resistivity values of ~ 450 to 130 Ω·m and a thickness up to 90 m. This layer is composed of two parts: one is found between TDEM soundings "T13" and "S-PUC-04" showing resistivity values of ~450 Ω·m and a thickness of up to 90 m, attributed to deposits from the middle part of the fan comprised of gravel and sand materials. The second part, located between soundings S-PUC-11 and S-PUC-10, shows resistivity values of ~200 Ω·m and a thickness of up to 90 m, are attributed as alluvial deposits from the distal part of the fan, consisting of sands and clays.

Below this layer, section S-PUC-12–S-PUC-10 shows a second layer with resistivity values of ~40-70 Ω·m and a thickness of ~60 to 130 m. This layer probably corresponds to deposits from the ancient Cabana and Mataro Lakes (Table 1). Higher values of resistivity (~70 Ω·m) might be attributed to the Mataro deposits, which are a series of fluviatile, detrital deposits showing alternating beds of clayey sand and gravelly sand (Table 1).

Profile 4

In Profile 4 (Fig.2, Fig.6), the sections located at 'Puerto Perez Bay 1' (i.e. soundings S24A to S32A) and at 'Puerto Perez Bay 2' (Fig. 6) provide more information about deposits from ancient lake invasions in the lower Piedmont area.

Sections located between soundings S24A-S32A and S28-S36 are characterized by a first layer with resistivity values of ~60 to 100 Ω·m and a thickness of 25 to 60 m, attributed to fluvio-lacustrine deposits (Qfl), which from borehole information corresponds to thin layered sequences comprising medium to coarse sand materials with

603 clay content. A second layer is observed between soundings S24 and S23 (~20 to 40
604 Ω·m) and a thickness of 20 m, that might correspond to deposits from the Mataro and
605 Cabana Lakes (Table 1).

606 Additionally, a change in resistivity values is observed immediately after section "S28-
607 S36". TDEM sounding S34 shows a first layer of resistivity of ~10 Ω·m and a thickness
608 of ~10 m, attributed to deposits from the Ballivian Lake, which from a nearby borehole
609 is comprised of clay deposits (BH-2, Fig. 4). Below this first layer, a second layer with
610 a resistivity value of ~30 Ω·m and a thickness of ~30 m, is attributed to the non-
611 differentiated Qcb-mt Formation (Table 1).

612 *Profiles 5 and 6*

613 Section S24A-S63 from Profile 5 (Fig.2 and Fig.6) shows additional information from
614 the lower Piedmont area. It shows resistivity values of ~60 to 100 Ω·m and a thickness
615 of ~20 to 40 m, which are attributed to fluvio-lacustrine deposits (Qfl). Below this first
616 layer, a second layer with resistivity values of ~30 to 40 Ω·m and a thickness of ~20 m,
617 is attributed as the non-differentiated Qcb-mt Formation. The same layer (Qcb-mt) is
618 observed in TDEM sounding S62A but with a thickness of ~80 m.

619 In addition, Profile 6 (Fig.2 and Fig.6) shows a first layer with resistivity values of ~60
620 Ω·m and a thickness of 20 to 40m, attributed to fluvio-lacustrine deposits (Qfl).
621 Immediately after, section S58-S56C, shows a layer with resistivity values of ~10 to 20
622 Ω·m and a thickness of ~7 to 20 m, which corresponds to clay deposits from the
623 Ballivian Lake (Qull) (Table 1).

624 The Tertiary or Devonian bedrock underlying the Quaternary deposits has conductive
625 values (Tlpz ~20Ω·m; Tpñ ~50Ω·m; Dclp ~15Ω·m) suggesting clay content and/or
626 fracturing for the Peñas (Tpñ) and Vila Vila Formations (Dvv), respectively (Table 1).

627 ***4.2.2.2 Lacustrine plain (lake invasions)***

628 *Profile 1*

629 Profile 1 (Fig.2, Fig.6) shows important information from the Lacustrine plain. From
630 NE to SW, ancient lakes invasions are illustrated in section P24-P2. In section P24-P5,
631 we find a first layer with resistivity values ~15 Ω·m and a thickness varying from 2 to

30 m, which correspond to deposits from Paleo-lake Ballivian "Ulloma Formation" (Qull) (Table 1). From borehole information, consists of fine sands with clayey and silty layers. The resistivity value of 15 Ω·m suggests that the clay content is significant.

A deeper second layer, found in sections (P24-P5) with resistivity values ~30 to 40 Ω·m and a thickness of 40 to 100 m, may belong to deposits from the ancient Lakes Cabana and Mataro, remaining as a unique non-differentiated formation (Qcb-mt) in this interpretation. Both formations are layered grounds with fluviatile indications (alternating clay, sand and gravel deposits) (Table 1).

Profile 3, 4 and 7

Additional information from the lacustrine plain is depicted in Profile 3 (Fig.2, Fig.7). The subterranean channel, investigated in section S-PUC-09–S-18A (E-W direction, Figure 7) shows resistivity values of ~40-70 Ω·m and a thickness of ~40 to 90 m, and is attributed to deposits from the ancient Cabana and Mataro Lakes, Qcb-mt (Table 1). This channel show deposits with lateral continuity interconnecting the Piedmont subsystem and the Lacustrine plain.

Section S-PUC-14–T6 (SE-NW direction) depicts a first layer with resistivity values of~10 Ω·m and a thickness of 5 to 30m, attributed to deposits from Paleo-lake Ballivian (Qull). Then, a second layer with resistivity values of ~45 Ω·m and a thickness of ~100 m is shown in section S-PUC-14–T4; this layer is attributed to the non-differentiated Qcb-mt deposits from the ancient Lakes Cabana and Mataro (Table 1).

The Lacustrine plain is also depicted in Profile 4 (Fig.6). Section S39-S43E shows a first layer with resistivity values of ~5 to 10 Ω·m and a thickness of ~7 to 45 m, attributed to deposits from Paleo-lake Ballivian (Qull), composed of clayey and silty layers (Table 1). Then, a second layer with resistivity values of ~35 to 45 Ω·m and a thickness of ~40 to 140 m may belong to the non-differentiated Qcb-mt Formation.

Profile 7 (Fig.6) provides more information from the Lacustrine plain. Section S44A-S48C shows a first layer with resistivity values of ~5 to 10 Ω·m and a thickness of ~30 to 45 m and is attributed to deposits from the ancient Ballivian Lake, Qull (Table 1). Below, a second layer is observed in sections S44A-T9, T11-S54, S48-S48C with

661 resistivity values of ~30 to 45 Ω·m and a thickness of 20 to 150 m, that may correspond
662 to deposits from the non-differentiated Cabana and Mataro Lakes (Qcb-mt).

663 Similarly to what was found for the Piedmont subsystem, the Quaternary paleo-
664 lacustrine deposits overlay the Tertiary or Devonian bedrock. Resistivity values (Tcl
665 ~150 Ω·m; Tkk ~40Ω·m; Dvv ~20 Ω·m; Dbl ~500 Ω·m) are considered to be the bottom
666 of the paleo-lacustrine geologic media.

667 ***4.3 Hydrogeochemical characteristics***

668 Groundwater in the Piedmont subsystem (blue and green circles, Fig.3 and Fig.8)
669 presents predominantly bicarbonate dominance with a noticeable increase of : i)
670 $Ca(Mg)$ relative to $Na(K)$ facies with EC ~$63 - 250 \mu S/cm$, and ii) $Na(K)$ relative to
671 $Ca(Mg)$ facies with EC ~$251 - 500\ \mu S/cm$.

672 The $Ca(Mg) - HCO_3^-$ facies relate silicate weathering from the Devonian/Silurian
673 sedimentary bedrock in the ancient fluvial-alluvial and glacial sedimentary
674 environments, while the $Na(K)$ enrichments result from groundwater mixing. Indeed,
675 TDEM results show that in the lower Piedmont fluvioglacial and alluvial layers (Qfg,
676 Qaa) overlay paleo-lacustrine layers (Qcb-mt). Therefore, groundwater hosted in the
677 Qfg, Qaa layers enriched in $\mathrm{Ca(Mg)} - \mathrm{HCO_3^-}$ flushes the evaporite enriched water in
678 exchangeable Na^+ hosted in the Qcb-mt layers.

679 Notably, enrichment trends of SO_4^{2-} and Cl^- facies with mixed $Na(K)$ and $Ca(Mg)$
680 contributions are attributed to: i) seepage from influent rivers, i.e. sulphate-rich
681 upstream waters locally influenced by environmental liabilities from inactive mines
682 (Fig. 3), or to ii) anthropogenic contamination from the urbanized areas of the city of El
683 Alto (Fig. 3).

684 Finally, groundwater in the lacustrine plain (cyan circles, Fig.3, Fig.8) is for some
685 sampling points enriched in $Na(K) - Cl^-$ facies (EC~$1690\ \mu S/cm$). These high
686 conductivity waters stand for the presence of evaporites originated from past
687 evaporation processes of lacustrine oirign. Relatively high HCO_3^- and SO_4^{2-}
688 concentrations *(*EC~$500\ to\ 700\ \mu S/cm$) are recorded for some samples located nearby
689 the outcropping bedrock, especially those close to the Kollu-Kollu Formation (Tkk;
690 Fig.1, Table 1).

691 ## 5. Discussion

692 ### *5.1 Extension and physical properties of the aquifer*

693 The aquifer extends from the Eastern Cordillera and is delimited by the most ancient
694 lake invasion "Lake Mataro" towards the southern, western and northern sides of the
695 Katari and Lago Menor Basin (Fig.9). According to Lavenu (1992) the top of the
696 Mataro deposits would be an ablation surface developed at a present-day altitude of
697 3,950 m a.s.l around the paleo-basin (see Fig.1 and topographic curves of Fig.2). The
698 limit of the aquifer towards the eastern side is delineated by the lower limit of rock
699 glaciers defined to be at approximately 4700 m a.s.l by Rangecroft et al. (2014) (Fig. 2).
700 More field work is required in the Achacachi region (Fig.1, Fig.2) because besides
701 glacial erosion, the topographic curve of 3,950 m a.s.l also suggests the influence of
702 ancient lake invasions and therefore could be part of the regional groundwater system.

703 The stratigraphic models presented in the results section are consistent with the
704 Quaternary sediments being hydraulically connected and behaving as a single regional
705 aquifer system. Continuity is locally disrupted when the substratum (Tertiary or
706 Devonian Formations) outcrops inside the domain.

707 The aquifer comprises: i) glacial (Qg) and fluvioglacial (Qfg) outwash layers of ~200 m
708 of thickness (above 4100 m a.s.l), in the upper Piedmont area, ii) fluvioglacial (Qfg) and
709 paleo-lacustrine layers (Qcb-mt), ranging from ~50 to 150 m of thickness, in the lower
710 Piedmont area, and iii) paleo-lacustrine layers (Qcb-mt) of ~40-150 m thickness in the
711 Lacustrine plain. A clay aquitard (Ulloma Formation, Qull), overlaying the paleo-
712 lacustrine layers (Qcb-mt) in the Lacustrine plain, presents a thickness of~45 meters
713 close to Lake Titicaca (Cohana bay) and decreases in thickness when far away from the
714 Lake (Fig.9, Fig.10).

715 In fact, a large portion of the aquifer presents an unconfined behaviour whereas it
716 remains confined below the Ulloma Formation (Fig.9, Fig.10). The thickness of the
717 unconfined portion varies from 50 to 150 meters and that of the confined from 100 to
718 150 meters. Values of hydraulic conductivity for the unconfined portion range from
719 $1.1 \times 10^{-4}\, m/sec$ (alluvial fan deposits, Qaa), $2.5 \times 10^{-6}\, m/sec$ (fluvioglacial
720 deposits, Qfg) to 5.9×10^{-8} m/sec (glacial deposits, Qg) (JICA, 1987; M.M.A.yA,

721 2016 ; Barroso, 2010), while for the confined part transmissivity values range around
722 6.0×10^{-6} m^2/sec (paleo-lacustrine deposits, Qcb-mt) (JICA, 1987).

723 ***5.2 Regional hydrogeological and geochemical functioning***

724 The groundwater flow system displayed in Fig.9 corresponds to a classical gravity-
725 driven regional groundwater flow (Tóth, 1999; Navarro de León et al., 2005; Tóth and
726 Hayashi, 2010; Mádl-Szönyi and Tóth, 2015). Regions with dashed potentiometric
727 contours were inferred from the combination of the interpreted geological, TDEM,
728 landscape and groundwater hydrochemical data.

729 Groundwater flow within the Katari and Lago Menor Basin is composed of several
730 interconnected groundwater flow systems (Fig.9). The main groundwater flow system
731 starts in the upper Piedmont (high mountain ranges of the Eastern Cordillera) and
732 follows the topographic Piedmont gradient (NE to SW) (Fig. 9 and Fig.10). Most
733 groundwater recharge results from the infiltration of precipitation and runoff on the high
734 mountain ranges. Indeed, groundwater circulating in the Piedmont layers (Qg, Qfg,
735 Qaa) show bicarbonate dominance with an enrichment of $Ca(Mg)$ facies (Fig.10).
736 However, when this type of water mixes with the evaporite enriched water of lacustrine
737 origin, $Na(K)$ is released.

738 The outcrops of the Devonian and Tertiary Formations within the Piedmont subsystem
739 (Fig.9 and Fig.10) act as underground barriers that deviate the flow to generate
740 individualised groundwater flow systems. Most of these groundwater flow systems
741 enter directly into Lake Titicaca (Puerto Perez Bays) and others reach the Lacustrine
742 plain. In contrast, the interruption of Quaternary deposits in the southern limit due to the
743 topographic depression (west of La Paz and Achocalla Cities) generates a natural
744 outflow of groundwater towards the hillsides of La Paz and Achocalla Cities.

745 The outcropping rock formations between the Piedmont subsystem and Lacustrine
746 plain, act as barriers that constrain the direction of the water flow, resulting in different
747 types of groundwater discharge in the lower Piedmont, particularly wetlands (Fig.9 and
748 Fig.10), where a large stock of groundwater is evaporated. According to Tóth (1999)
749 and Tóth and Hayashi (2010) these typical hydrologic features also result from the
750 action of groundwater moving in basin-scale gravity-flow systems.

751 Finally, the groundwater flow systems that reach the Lacustrine plain and the
752 groundwater flow system starting in the Collana limit (Fig.1, Fig.9) follow the SE-NW
753 topographic gradient towards Lake Titicaca (Cohana Bay). Groundwater hosted in the
754 Qcb-mt layers probably moves further since the present Lake Titicaca overlays deposits
755 from Paleo-lake Ballivian "Ulloma Formation, Qull" (Fig.9 and Fig.10) and these
756 deposits overlay the Qcb-mt deposits.

757 In the Lacustrine plain, groundwater hosted in the paleo-lacustrine layers (Qcb-mt),
758 underlying the clay aquitard (Qull, Ulloma Formation) presents predominantly
759 $Na(K) - Cl^-$facies relating the presence of evaporites. The presence of this aquitard
760 may retard dissolution processes of these soluble minerals due to low infiltration rates
761 of meteoric waters or any contaminants as it is attested by the high electrical
762 conductivity values in this area (~1690 µS/cm). Additionally, the increases of HCO_3^-
763 and SO_4^{2-} anions can relate to ancient processes that favoured the erosion of Tertiary
764 Formations containing evaporitic rocks such as the Kollu-Kollu Formation (Tkk ; Table
765 1) which is composed of evaporitic layers (limestone and gypsum) at the top of the
766 formation (Zeballos et al., 2017). In fact, Quino et al. (2019) reported the same
767 hydrogeochemical patterns in groundwater samples located close to the Tkk Formation.

768 **6. Conclusions and final recommendations**

769 This paper presents a multidisciplinary study using geology, geophysics (TDEM),
770 geochemistry, and groundwater level measurements for the assessment of a large scale
771 aquifer within the Katari and Lago Menor Basin, located in the semi-arid Altiplano,
772 between the Eastern Cordillera and the south-east of Lake Titicaca. This study gives a
773 first insight of the 3D geometry and the geochemical and hydrogeological functioning
774 of the Katari-Lago Menor Basin aquifer. Some of the necessary information for further
775 sustainable management of this aquifer, such as geometry and extent of the domain,
776 physical parameters and boundary conditions, are now available.

777 Time Domain Electromagnetics (TDEM) was found as an efficient method for
778 identifying the subsurface structure of the different geological formations present in the
779 study area, within the range of 0 to 200 m depth. Resistivity profiles combined with
780 geology, borehole lithology, topography as well as additional groundwater level and
781 geochemical measurements, were helpful in resolving the spatial limits of the aquifer,

782 the vertical and lateral continuity of the Quaternary porous geologic media, the shape
783 and position of the bottom of the aquifer (depth to the bedrock, i.e. Tertiary or Devonian
784 Formations), and revealed a general overview of the natural dynamic behaviour of the
785 aquifer at the scale of the Katari and Lago Menor Basin.

786 The stratigraphic models were consistent with the Quaternary sediments being
787 hydraulically connected and behaving as a single regional aquifer system. The main
788 groundwater flow system starts in the upper Piedmont, follows the topographic
789 Piedmont gradient (NE to SW) and discharges in a series of wetlands. Part of the
790 groundwater flow that reaches the Lacustrine plain follows the SE-NW topographic
791 gradient towards Lake Titicaca (Cohana Bay).

792 The next step is the development of a 3D numerical groundwater flow model to
793 improve the understanding of the whole groundwater flow system in this aquifer. The
794 building of this model also could be facilitated by denser electromagnetic TDEM
795 surveys (ground based or airborne). This model will be a powerful tool for the
796 sustainable management of groundwater resources. Such type of model will help in
797 evaluating and quantifying the groundwater resources and test different groundwater
798 development scenarios including pollution problems.

799 **Acknowledgments**

800 The present study was undertaken with the financial support of the Plurinational State of
801 Bolivia provided through the Program “100 Scholarships for Postgraduate Education
802 within the Framework of Technological and Scientific Sovereignty”, Supreme Decree
803 2100 (1 September 2014) and administered by the Ministry of Education (MINEDU).
804 And partly funded by LABEX OSUG@2020, ANR grant no.ANR-10-LABX-56
805 (financed by the Future Investments programme launched by the French government
806 and implemented by the ANR). We would like to thanks to the Ministry of Environment
807 and Water (M.M.A.yA, La Paz) and the University of San Andres (UMSA, La Paz) for
808 their logistical and technical support. Special thanks to Marizol Flores, Elise Levasseur,
809 Enrique and Mr. Julio César Salinas for their assistance in the field work, to the IGE
810 laboratory for their technical assistance and support during the analysis of the water
811 samples, and to the local communities of the Municipalities of Pucarani, Batallas, Laja,
812 Viacha, Puerto Pérez and El Alto for their support during the field work.

References

Abbott, M.B., Wolfe, B.B., Wolfe, A.P., Seltzer, G.O., Aravena, R., Mark, B.G., Polissar, P.J., Rodbell, D.T., Rowe, H.D., Vuille, M., 2003. Holocene paleohydrology and glacial history of the central Andes using multiproxy lake sediment studies. Palaeogeography, Palaeoclimatology, Palaeoecology 194, 123-138.

Achá, D., Guédron, S., Amouroux, D., Point, D., Lazzaro, X., Fernandez, P.E., Sarret, G., 2018. Algal Bloom Exacerbates Hydrogen Sulfide and Methylmercury Contamination in the Emblematic High-Altitude Lake Titicaca. Geosciences 8, 438.

Agramont, A., Craps, M., Balderrama, M., Huysmans, M., 2019. Transdisciplinary Learning Communities to Involve Vulnerable Social Groups in Solving Complex Water-Related Problems in Bolivia. Water 11, 385.

Araos, J.M., Le Roux, J.P., Gutierrez, N.M., 2017. Relict glacial landscape in the Sierra Baguales Mountain Range (50°-51° S): evidence of glaciation dynamics and types in the eastern foothills of the southern Patagonian Andes. J. Mt. Sci. 14(2): 282-295.

Archundia, D., Duwig, C., Spadini, L., Uzu, G., Guedron, S., Morel, M.C. 2017a. How Uncontrolled Urban Expansion Increases the Contamination of the Titicaca Lake Basin (El Alto, La Paz, Bolivia). Water Air And Soil Pollution 228, 44.

Archundia, D., Duwig, C., Lehembre, F., Chiro,n S., Morel, M.C., Prado, B., Bourdat-Deschamps, M., Vince, E., Flores Aviles, G., Martins, J.M.F., 2017b. Antibiotic pollution in the Katari subcatchment of the Titicaca Lake: major transformation products and occurrence of resistance genes. Science of the Total Environment 576, 671–682.

Argollo, J., Mourguiart, P. 1995. Los Climas Cuaternarios de Bolivia. Cambios Cuaternarios en América del Sur. In: JArgollo, J., Mourguiart, P. (Eds.), Climas Cuaternarios en América del Sur. ORSTOM-UMSA, 135-155.

841 Argollo, J., Mourguiart, P., 2000. Late Quaternary climate history of the Bolivian
842 Altiplano. Quaternary International 72, 37-51.

843 Argollo J, Iriondo M (2008) El Cuaternario de Bolivia y Regiones vecinas. Ed.: Moglia
844 (ISBN 9872463700), 280 pages.

845 Auken, E., Christiansen, A. V., Jacobsen, B.H., Foged, N., Sørensen, K.I., 2005.
846 Piecewise 1D laterally constrained inversion of resistivity data, 2005. Geophysical
847 Prospecting 53 (4), 497-506.

848 Ballivian, O., Bles, J.E., Servant, M., 1978. El Plio-Cuaternario de la Región de La Paz
849 (Andes Orientales, Bolivia). Cah. O.R.S.T.O.M. sér. Géol. 10 (1), 101–113.

850 Barroso, C.A., 2010. Delimitación de la contaminación del agua subterránea por
851 lixiviados en un till glacial del relleno sanitario "Villa Ingenio": El Alto-Bolivia.
852 Universidad Mayor Real Pontificia de San Francisco Xavier de Chuquisaca. Tesis
853 de Posgrado.

854 B.I.D., 2016. Programa de Saneamiento del Lago Titicaca (Cuenca Katari, Bahía
855 Cohana) BO-L1118. Marco de Gestión Ambiental y Social (MGAS), 87 pp.

856 Bush, M.B., Hanselman, J.A., Gosling, W.D., 2010. Nonlinear climate change and
857 Andean feedbacks: an imminent turning point? Global Change Biology 16 (12),
858 3223-3232.

859 Canedo, C., Pillco, Z.R., Berndtsson, R., 2016. Role of Hydrological Studies for the
860 Development of the TDPS System. Water 8(4), 144.

861 Condom, T., Coudrain, A., Dezetter, A., Brunstein, D., Delclaux, F., Sicart, J.E., 2004.
862 Transient modelling of lacustrine regressions: two case studies from the Andean
863 Altiplano. Hydrol. Process. 18, 2395–2408.

864 Cross, S., Baker, P., Seltzer, G., Fritz, S., Dunbar, R., 2001. Late Quaternary Climate
865 and Hydrology of Tropical South America Inferred from an Isotopic and
866 Chemical Model of Lake Titicaca, Bolivia and Perú. Quaternary Research 56(1),
867 1-9.

868 Coudrain-Ribstein, A., Olive, P., Quintanilla, J., Sondag, F., Cahuaya, D., 1995. Salinity
869 and isotopic dynamics of the groundwater resources on the Bolivian Altiplano.
870 Application of Tracers in Arid Zones Hydrology, Proceedings of the Vienna
871 Symposium. IAHS Publ. 232, 267-276.

872 Descloitres, M., Chalikakis, K., Legchenko, A., Moussa, A.M., Genthon, P., Favreau,
873 G., Le Coz, M., Boucher, M., Oï, M., 2013. Investigation of groundwater
874 resources in the Komadugu Yobe Valley (Lake Chad Basin, Niger) using MRS
875 and TDEM methods. Journal of African Earth Sciences 87, 71–85.

876 Emmer, A., Juřicová, A., Veettil, B.K., 2019. Glacier retreat, rock weathering and the
877 growth of lichens in the Churup Valley, Peruvian Tropical Andes. J. Mt. Sci.
878 16(7), 1485-1499.

879 Fernandes, A.J., Maldaner, C.H., Negri, F., Rouleau, A., Wahnfried, I.D. 2016. Aspects
880 of a conceptual groundwater flow model of the Serra Geral basalt aquifer (Sao
881 Paulo, Brazil) from physical and structural geology data. Hydrogeol. J. 24, 1199–
882 1212.

883 Fitterman, D.V., Stewart, M.T., 1986. Transient electromagnetic sounding for
884 groundwater. Geophysics 51(4), 995-1005.

885 Foster, S., Koundouri, P., Tuinhof, A., Kemper, K., Nanni, M., Garduno, H., 2006.
886 Groundwater dependent ecosystems: the challenge of balanced assessment and
887 adequate conservation. GW Mate briefing note series; no. 15. Washington, DC:
888 World Bank. http://documents.worldbank.org/curated/en/407851468138596688

889 Fritz, S.C., Baker, P.A., Lowenstein, T.K., Seltzer, G.O., Rigsby, C.A., Dwyer, G.S.,
890 Tapia, P.M., Arnold, K.K., Ku, T.L., Luo, S., 2004. Hydrologic variation during
891 the last 170,000 years in the southern hemisphere tropics of South America.
892 Quaternary Research 61, 95– 104.

893 Fritz, S.C., Baker, P.A., Tapia, P., Garland, J., 2006. Spatial and temporal variation in
894 cores from Lake Titicaca, Bolivia/Peru during the last 13,000 years. Quaternary
895 International 158(1), 23-29.

Fritz, S.C., Baker, P.A., Seltzer, G.O., Ballantyne, A., Tapia, P., Cheng, H., Edwards, R.L., 2007. Quaternary glaciation and hydrologic variation in the South American tropics as reconstructed from the Lake Titicaca drilling project. Quaternary Research 68 (3), 410-420.

Garcia, M.E., Bengtsson, L., Persson, K.M., 2010. On the distribution of saline groundwater in the Poopó Basin, Central Bolivian Highland. Journal of Water Management and Research 66, 199–203.

Geerts, S., Raes, D., Garcia, M., Taboada, C., Miranda, R., Cusicanqui, J., Mhizha, T., Vacher, J., 2009. Modeling the potential for closing quinoa yield gaps under varying water availability in the Bolivian Altiplano. Agricultural Water Management 96, 1652–1658.

GEOSIRH, 2017. Infraestructura de Datos Espaciales. Plan Director de la Cuenca Katari y Lago Menor del Titicaca. Ministerio de Medio Ambiente y Agua. Viceministerio de Recursos Hídricos y Riego.http://geosirh.riegobolivia.org/layers/geosirh.

GEOBOL, 1995. Geological sheets Calamarca N° 5943, Jesús Macha N° 5843, Tiahuanacu N°5844, La Paz N°5944, Achacachi N°5845 and Milluni N°5945 Escala 1:100000, Servicio Geologico de Bolivia (GEOBOL) and Geological Swedish AB (eds).

Gómez, E., Barmen, G., Rosberg, J., 2016. Groundwater Origins and Circulation Patterns Based on Isotopes in Challapampa Aquifer, Bolivia. Water 8, 207.

Gómez, E., Larsson, M., Dahlin, T., Barmen, G., Rosberg, J.E., 2019. Alluvial aquifer thickness and bedrock structure delineation by electromagnetic methods in the highlands of Bolivia. Environmental Earth Sciences 78, 84.

Gonzales Amaya, A., Ortiz, J., Durán, A., Villazón, M., 2018a. Hydrogeophysical methods and hydrogeological models: basis for groundwater sustainable management in Valle Alto (Bolivia) . Sustainable Water Resources Management 5(3), 1179-1188.

924 Gonzales Amaya, A., Mardh, J., Dahlin, T., 2018b. Delimiting a saline water zone in
925 Quaternary fluvial–alluvial deposits using transient electromagnetic: a case study
926 in Punata, Bolivia. Environmental Earth Sciences 77,46.

927 Guédron, S., Point, D., Acha, D., Bouchet, S., Baya, P.A., Tessier, E., Monperrus, M.,
928 Molina, C.I., Groleau, A., Chauvaud, L., Thebault, J., Amice, E., Alanoca, L.,
929 Duwig, C., Uzu, G., Lazarro, X., Bertrand, A., Bertrand, S., Barbraud, C., Delord,
930 K., Gibon, F.M., Ibanez, C., Flores, M., Fernandez Saavedra, P., Ezpinoza, M.E.,
931 Heredia, C., Rocha, F., Zepita, C., Amouroux, D., 2017. Mercury contamination
932 level and speciation inventory in Lakes Titicaca & Uru-Uru (Bolivia): Current
933 status and future trends. Environmental Pollution 231, 262-270.

934 Guérin, R., Descloitres, M., Coudrain, A., Talbi, A., Gallaire, R., 2001. Geophysical
935 surveys for identifying saline groundwater in the semi-arid region of the central
936 Altiplano, Bolivia. Hydrological Processes 15, 3287–3301.

937 Harrington, J.S., Mozil, A., Hayashi, M., Bentley, L.R., 2018. Groundwater flow and
938 storage processes in an inactive rock glacier. Hydrological processes. doi:
939 10.1002/hyp.13248.

940 Heine, K., 2004. Late Quaternary Glaciations of Bolivia. Quaternary Glaciations-Extent
941 and Chronology 2(C), 83–88.

942 JICA, 1987. Final Report for the Study on groundwater development Project on El Alto
943 district in La Paz city. Japan International Cooperation Agency. Republic of
944 Bolivia.

945 Jones, D.B., Harrison, S., Anderson, K., Whalley, W.B., 2019. Rock glaciers and
946 mountain hydrology: A review. Earth-Science Reviews, 193, 66-90.

947 Kinouchi, T., Liu, T., Mendoza, J., Asaoka, Y., 2013. Modeling glacier melt and runoff
948 in a high-altitude headwater catchment in the Cordillera Real, Andes. Hydrol.
949 Earth Syst. Sci. Discuss., 10, 13093–13144.

950 Kinouchi, T., Nakajima, T., Mendoza, J., Fuchs, P., Asaoka, Y., 2019. Water security in
951 high mountain cities of the Andes under a growing population and climate
952 change: A case study of La Paz and El Alto, Bolivia. Water Security 6, 100025.

953 Lamb, S., Hoke, L., 1997. Origin of the high plateau in the Central Andes, Bolivia,
954 South America. Tectonics 16(4), 623-649.

955 Lavenu, A., 1992. Formation and geological evolution. In: Dejoux, C., Iltis, A. (Eds.),
956 Lake Titicaca: A Synthesis of Limnological Knowledge, Kluver Academic
957 Publishers, pp. 3-13.

958 Mádl-Szönyl, J., Tóth, Á., 2015. Basin-scale conceptual groundwater flow model for an
959 unconfined and confined thick carbonate region. Hydrogeol. J. 3, 1359–1380.

960 Maldonado, L., Bécher, F., Cabrera, A., Blarasina, M., Lutria, V., Matteoda, E.,
961 Giuliano, J., 2018. Hydrogeochemical features and groundwater renewal rate
962 estimates from deep aquifers in the Pampean plain, Córdoba province, Argentina.
963 Journal of South American Earth Sciences 85, 126–134.

964 Melly, B.L., Schael, D.M., Gama, P.T., 2017. Perched wetlands: An explanation to
965 wetland formation in semi-arid areas. Journal of Arid Environments 141, 34-39.

966 Mira, A., Veroslavsky, G., Rossello, E., Vives, L., 2015. Subsurface geological
967 modeling of Corrientes province (NE Argentina) and its relationships with the
968 Guaraní Aquifer system function. Journal of South American Earth Sciences 62,
969 148-163.

970 Murray, B.P., Horton, B.K., Matos, R., Heizler, M.T., 2010. Oligocene–Miocene basin
971 evolution in the northern Altiplano, Bolivia: Implications for evolution of the
972 central Andean backthrust belt and high plateau. GSA Bulletin 122(9/10), 1443–
973 1462.

974 M.M.A.yA., 2014. Plan Maestro Metropolitano de Agua Potable y Saneamiento La Paz
975 - El Alto, Bolivia. Ministerio de Medio Ambiente y Agua, Viceministerio de
976 Recursos Hídricos y Riego, La Paz, Bolivia, 932 pp.

977 M.M.A.yA., 2016. Plan de Manejo Preliminar de los Acuíferos de Purapurani y Viacha.
978 Ministerio de Medio Ambiente y Agua, Viceministerio de Recursos Hídricos y
979 Riego, La Paz, Bolivia, 184 pp.

Navarro de León, I., Gárfias-Soliz, J., Mahklnecht, J., 2005. Groundwater flow regime under natural conditions as inferred from past evidence and contemporary field observations in a semi-arid basin: Cuenca de la Independencia, Guanajuato, México. Journal of Arid Environments 63, 756–771

N.A.S.A, 2000. Shuttle Radar Topography Mission (SRTM) 1 Arc-Second Global, project from the National Aeronautics and Space Administration. Available at http://dds.cr.usgs.gov/ee-data/coveragemaps/shp/ee/srtm/srtm.zip

Pauritsch, M., Wagner, T., Winkler, G., Birk, S., 2017. Investigating groundwater flow components in an Alpine relict rock glacier (Austria) using a numerical model. Hydrogeol. J. 25, 371–383.

Placzek, C.J., Quade, J., Patchett, P.J., 2011. Isotopic tracers of paleohydrologic change in large lakes of the Bolivian Altiplano. Quaternary Research 75, 231–244.

Oyarzún, R.. Barrera, F., Salazar, P., Maturama, H., Oyarzún, J., Aguirre, E., Alvarez, P., Jourde, H., Kretschmer, N., 2014. Multi-method assessment of connectivity between surface water and shallow groundwater: the case of Limarí River basin, north-central Chile. Hydrogeol. J. 22, 1857–1873.

Quesada, B., Sylvestre, F., Vimeux, F., Black, J., Paillès, C., Sonzogni, C., Alexandre, A., Blard, P.H., Tonetto, A., Mazur, J.C., Bruneton, H., 2015. Impact of Bolivian paleolake evaporation on the δ18O of the Andean glaciers during the last deglaciation (18.5-11.7 ka): diatom-inferred δ18O values and hydro-isotopic modeling. Quaternary Science Reviews 120, 93-106.

Quino, L.I., Ormachea, M.M., Ramos Ramos, O.E., Bhattacharya, P., Quispe, C.R., Quintanilla, A.J., Sracek, O., 2019. Hydrochemical assessment with respect to arsenic and other trace elements in the Lower Katari Basin, Bolivian Altiplano. Groundwater for Sustainable Development 8, 281–293.

Rabatel, A., Francou, B., Soruco, A., Gomez, J., Caceres, B., Ceballos, J.L., 2013. Current state of glaciers in the tropical Andes: a multi-century perspective on glacier evolution and climate change. Cryosphere 7(1), 81–102.

1008 Ramos Ramos, O.E., 2014. Geochemistry of trace elements in the Bolivian Altiplano-
1009 Effects of natural processes and anthropogenic activities. PhD Thesis, Royal
1010 Institute of Technology in Stockholm, Universidad Mayor de San Andrés La Paz,
1011 68 pp.

1012 Rangecroft, S., 2014. Rock glaciers, water security and climate change in the Bolivian
1013 Andes. PhD thesis, University of Exeter, 318 pp.

1014 Rangecroft, S., Suggitt, A.J., Anderson, K., Harrison, S., 2016. Future climate warming
1015 and changes to mountain permafrost in the Bolivian Andes. Climatic Change 137
1016 (1-2), 231-243.

1017 Salvaderry - Aranguren, M.M., Probst, A., Roulet, M., Isaure, M.P., 2008.
1018 Contamination of surface waters by mining wastes in the Milluni Valley
1019 (Cordillera Real, Bolivia): Mineralogical and hydrological influences. Applied
1020 Geochemistry 23(5), 1299-1324.

1021 Sánchez-Saldías, A., Fariña, R.A., 2014. Palaeogeographic reconstruction of Minchin
1022 palaeolake system, South America: The influence of astronomical forcing.
1023 Geoscience Frontiers 5, 249-259.

1024 Satge, F., Denezine, M., Pillco, R., Timouk, F., Pinel, S., Molina, J., Garnier, J., Seyler,
1025 F., Bonnet, M.P., 2016. Absolute and relative height-pixel accuracy of SRTM-
1026 GL1 over the South American Andean Plateau. ISPRS Journal Photogrammetry
1027 and Remote Sensing 121, 157–166.

1028 Simler, R., 2014. Manuel d'utilisation DIAGRAMMES. Pages 1-42

1029 Soruco, A., Vincent, C., Rabatel, A., Francou, B., Thibert, E., Sicart, J., & Condom, T.
1030 (2015). Contribution of glacier runoff to water resources of La Paz city, Bolivia
1031 (16° S). Annals of Glaciology, 56(70), 147-154.

1032 Suárez-Soruco, R., Díaz-Martínez, E., 1996. Léxico Estratigráfico de Bolivia. Revista
1033 Técnica de Yacimientos Petrolíferos Fiscales Bolivianos, 17(1-2), 3-227.

1034 Sugaki, A., Kitakaze, A., 1988. Tin-bearing Minerals from Bolivian Polymetallic
1035 Deposits and their Mineralization Stages. Mining Geology 38(5), 419-435.

1036 Tóth, J., 1999. Groundwater as a geologic agent: An overview of the causes, processes,
1037 and manifestations. Hydrogeol. J. 7, 1–14.

1038 Tóth, J., Hayashi M., 2010. The theory of basinal gravity flow of groundwater and its
1039 impacts on hydrology Japan. J. Groundwater Hydrol. 52, 335-354.

1040 Uribe, J., Muñoz, J.F., Gironás, J., Oyarzún, R., Aguirre, E., Aravena, R., 2015.
1041 Assessing groundwater recharge in an Andean closed basin using isotopic
1042 characterization and a rainfall-runoff model: Salar del Huasco basin, Chile.
1043 Hydrogeol. J. 23: 1535–1551.

1044 Viguier, B., Jourde, H., Yáñez, G., Lira, E., Leonardi, V., Moya, C., García-Pérez, T.,
1045 Maringue, J., Lictevout, E., 2018. Multidisciplinary study for the assessment of
1046 the geometry, boundaries and preferential recharge zones of an overexploited
1047 aquifer in the Atacama Desert (Pampa del Tamarugal, Northern Chile). J. South
1048 Am. Earth Sci. 86, 366–383.

1049 Veettil, B.K., Wang, S., Simões, J.C., Ruiz Pereira, S.F., 2018. Glacier monitoring in
1050 the eastern mountain ranges of Bolivia from 1975 to 2016 using Landsat and
1051 Sentinel-2 data. Environ. Earth Sci. 77, 452.

1052 Winkler, G., Wagner, T., Pauritsch, M., Birk, S., Kellerer-Pirklbauer, A., Benischke, R.,
1053 Leis, A., Morawctz, R., Schreilechner, M.G., Hergarten, S., 2016. Identification
1054 and assessment of groundwater flow and storage components of the relict
1055 Schöneben Rock Glacier, Niedere Tauern Range, Eastern Alps (Austria).
1056 Hydrogeol. J. 24, 937–953.

1057 Zeballos, A., Weihd, P., Blanco, M., Machaca, V., 2016. Geological, mineralogical and
1058 chemical characterization of Devonian kaolinite-bearing sediments for further
1059 applications in the ceramic (tiles) industry in La Paz, Bolivia. Environ. Earth Sci.
1060 75, 546.

1061 Zeballos, A., Weihd, P., Blanco, M., Machaca, V., 2017. Characterization of some
1062 nonmetallic resources in Bolivia: an overview of their potentiality and their
1063 application in specialized formulations. Environ. Earth Sci. 76, 754.

1064 Zech, R., Kull, C., Kubik, P.W., Veit, H., 2007. LGM and Late Glacial glacier advances
1065 in the Cordillera Real and Cochabamba (Bolivia) deduced from 10Be surface
1066 exposure dating. Clim. Past, 3, 623–635.

Table 1. Lithostratigraphy of the study area (literature review Ballivian, 1978; Lavenu, 1992; GEOBOL & Swedish Geological AB, 1995; Suárez-Soruco and Díaz-Martínez, 1996; Argollo and Mourguiart, 2000; Heine, 2004; Argollo and Iriondo 2008; Fritz et al., 2004; Salvaderry-Aranguren et al., 2008; Murray et al., 2010; Sánchez-Saldías and Fariña, 2014; Zeballos et al., 2016 ; Zeballos et al., 2017).

			Piedmont subsystem[1]			**Lacustrine plain**		
System	**Epoch**	**Quaternary Glaciations**	**Formation/Deposit**	**Symbol**	**Lithology**	**Formation/Deposit**	**Symbol**	**Lithology**
Quaternary	Holocene		Alluvial deposits	Qaa*	Pebbles, gravels, sand and silt	Fluvio lacustrine deposits	Qfl	Gravels, sands, silt and clay
						Deposits (Lake Titicaca)	Ql	Silts, clays and sands
			Low Terrace			*Erosion surface*		Evaporites
			High Terrace	Qt	Pebbles, gravel, sand, silt and clay	Deposits (Paleo-lake Tauca)		No influence in the Northern Altiplano
	Upper Pleistocene	Choqueyapu Glaciation (Stage 2)	Choqueyapu II Formation	Qg	(Frontal moraines)			
						Deposits (Paleo-Lake Minchin)		No influence in the Northern Altiplano
		Choqueyapu Glaciation (Stage 1)	Choqueyapu I Formation	Qg	(Lateral moraines)	*Erosion surface*		Alluvial/Colluvial - Dunes deposits
			Ablation surface		Gravels and soils (fluvial erosion)			
						Ulloma Fm.(Deposits from Pale-lake Ballivian)	Qull	Well stratified fine sands with an alternation of clayey and silty layers
		Sorata Glaciation	Sorata Formation	Qg	Moraine ridges and flow-tills (clasts and blocks of quarzites, shales and granites in a clayey matrix)			
			Ablation Surface		Gravel and soils (red horizon with iron accumulations)*			
						Paleo-lacustrine deposits (Paleo-lake Cabana)	Qcb-mt	Clay and sand laminae with banks of gravels and sands ~50m thickness (presence of halite/gypsum evaporites)
	Lower Pleistocene	Kaluyo Glaciation	Kaluyo Formation	Qg	Tills composed of striated rock blocks with an intercalation of fluvio-glacial gravels			
			Purapurani Formation	Qfg	Conglomerates with rounded elements (Upper part) and gravels in a clayey matrix with paleo-soil levels and clayey intercalations (Lower part)	Paleo-lacustrine deposits from Paleo-lake Mataro		Alternation of clay-sandy banks and sand-gravelly layers ~50m thickness (presence of halite/gypsum evaporites)
		Calvario glaciation	Calvario Formation	Qg	Tills of gravels and blocks (mainly granites) in a silty-sandy matrix. The upper part of this till presents fluvial gravels			
			Precalvarian Deposits		Gravels			
			Erosion Surface		Red paleo-soil			

***** Alluvial fan deposits (Qaa) could also represent a significant accumulation of Pre-Sorata gravels (Argollo and Iriondo, 2008)

[1] Ancient lake invasions could have reached the lower Piedmont area (Lavenu, 1992). Therefore, paleo-lacustrine deposits could underlay Pleistocene glacial and/or fluvioglacial eposits.

Table 1, Continued

Tertiary	Pliocene	La Paz Formation	Tlp Fm.	Clay-sandy well stratified deposits with different levels of cinerita tuff	Taraco Formation	Ttc	Red-orange conglomerates and sandstones
	Upper Miocene	Cachilaya Formation	Tcl Fm.	Polymictic conglomerates, claystones with tuff levels			
	Lower Miocene-Upper Oligocene	Kollu Kollu Formation	Tkk Fm.	Series of gypsum-bearing sandstones and claystones of lacustrine facies (evaporitic layers to the top)	Kollu Kollu Formation	Tkk	Series of gypsum-bearing sandstones and claystones of lacustrine facies (evaporitic layers at the top of the Formation)
		Peñas Formation	Tpñ Fm.	Reddish polymorphic conglomerates and sandstones	Coniri Formation	Tcnr	Reddish polymorphic conglomerates and sandstones
Devonian	Late-Middle	Colpacucho Formation	Dclp Fm.	Shales and finely stratified siltstones and powerful sandstone banks			
	Early	Belen Formation	Dbl Fm.	Alternation of fine-grained sandstone and shabby grayish-black shales	Belen Formation	Dbl	Alternation of fine-grained sandstone and shabby grayish-black shales
		Vila Vila Formation	Dvv Fm.	Sandstones and quartize banks of medium grain with crossed stratification (highly weathered siltstones)	Vila Vila Formation	Dvv	Sandstones and quartize banks of medium grain with crossed stratification (highly weathered siltstones)
Silurian	Pridoli	Catavi Formation	Sct Fm.	Black shales and sandstones deformed by faults and folds			

Table 2. Location of TDEM soundings and investigated formations. The location is based on the UTM WGS84 zone 19S coordinate system. The altitude values are based on SRTM-GL1-30m. Coincident loop configuration Tx=Rx : (loop size in meters).

	ID	Easting (m)	Northing (m)	Surface Altitude SRTM (m a.s.l)	Tx (m)	Rx (m)	Investigated formations
Profile 1							
1	S0-A	582720	8193215	4658	100	100	
2	S3-A	582153	8192355	4609	100	100	
3	S5-A	581576	8191530	4511	100	100	
4	S2-A	581074	8190309	4411	100	100	
5	S4-A	580869	8189419	4379	100	100	
6	S1-A	580356	8188442	4312	100	100	Glacial/ fluvioglacial deposits
7	S11-A	580188	8186907	4222	100	100	
8	S8-A	578872	8186472	4187	100	100	
9	S8-B	578629	8185885	4160	100	100	
10	S10-A	577521	8185608	4121	100	100	
11	S7-A	576258	8184721	4077	100	100	
12	S9-A	575328	8183866	4041	100	100	
13	S-PUC-07	574191	8183280	4009	100	100	
14	S-PUC-06	573081	8182707	3982	100	100	
15	**P1-17**	572142	8182223	3957	100	100	
16	P64	571147	8181522	3938	100	100	
17	P63	570674	8181093	3922	100	100	
18	P62	570169	8180758	3914	100	100	Alluvial/ paleo-lacustrine deposits
19	P61	569904	8180227	3907	100	100	
20	P60	569607	8179763	3899	100	100	
21	P59	569324	8179153	3893	100	100	
22	P58	568901	8178541	3885	100	100	
23	P57	568776	8178016	3884	100	100	
24	P56	568427	8177333	3878	100	100	
25	P55	567885	8176845	3906	100	100	
26	P54	567607	8176423	3921	100	100	
27	P53	567188	8175795	3886	100	100	Tertiary Formation (Tcl)
28	P52	567284	8175262	3902	100	100	
29	P51	566727	8174943	3883	100	100	
30	P50	566304	8174582	3868	100	100	
31	P49	565880	8174310	3849	100	100	
32	P48	565785	8174042	3851	100	100	
33	P47	565602	8173791	3852	100	100	
34	P46	565461	8173765	3851	100	100	
35	P45	565458	8173493	3852	100	100	Paleo-lacustrine deposits
36	P44	565388	8173200	3853	100	100	
37	P43	565079	8173092	3858	100	100	
38	P42	564938	8172616	3852	100	100	
39	S-LJ-01	564441	8171993	3844	100	100	
40	P39	563690	8171570	3878	25	25	
41	P38	563640	8171541	3876	25	25	Devonian Formation (Dbl)
42	P37	563600	8171526	3873	25	25	
43	P36	563513	8171503	3856	25	25	
44	P34	563468	8171486	3847	25	25	
45	P32	563377	8171464	3845	25	25	Paleo-lacustrine deposits
46	P31	563340	8171481	3843	25	25	

Table 2, Continued

	ID	Easting (m)	Northing (m)	Surface Altitude SRTM (masl)	Tx (m)	Rx (m)	Investigated Formations
Profile 1							
47	P30	563283	8171501	3839	25	25	
48	P29	563185	8171473	3842	25	25	
49	P27	562890	8171391	3845	100	100	
50	P26	562323	8171504	3846	50	50	
51	P25	561881	8170585	3867	100	100	
52	P24	561170	8169978	3854	100	100	
53	P23	560260	8169988	3856	100	100	Paleo-lacustrine deposits
54	P22	559434	8169828	3858	100	100	
55	S-LJ-04	559507	8168884	3856	100	100	
56	P21	559793	8169370	3856	100	100	
57	P20	559060	8168386	3843	100	100	
58	P19	558692	8168452	3842	25	25	
59	P18	558683	8168402	3843	25	25	
60	P17	558646	8168280	3843	25	25	
61	P16	558665	8168232	3842	100	100	
62	P15	558603	8168230	3841	25	25	
63	P14	558483	8168183	3841	25	25	
64	P13	558430	8168169	3841	25	25	
65	P12	558421	8168156	3841	100	100	Paleo-lacustrine deposits
66	P11	558391	8168139	3840	25	25	
67	P10	558348	8168110	3841	25	25	
68	P8	558051	8167758	3848	100	100	
69	P7	557924	8167574	3860	100	100	
70	P6	557455	8167072	3856	100	100	
71	P5	556978	8166905	3859	100	100	
72	P4	556683	8166718	3883	100	100	Tertiary Formation (Tkk)
73	P3	556515	8166626	3907	100	100	
74	P2	555528	8166074	3869	100	100	Paleo-lacustrine deposits
75	P1	555105	8165863	3894	100	100	Tertiary Formation (Tcnr)
Profile 2							
76	**T-13**	558610	8194231	3933	100	100	
77	T-14	560008	8193393	3941	100	100	
78	T-15	561508	8192215	3951	100	100	
79	P1-23	562806	8191192	3956	100	100	
80	S13	563888	8190422	3965	100	100	Alluvial deposits (Major alluvial fan)
81	S-PUC-21	564641	8189691	3960	100	100	
82	S14	565312	8189056	3953	100	100	
83	S15	566385	8187983	3941	100	100	
84	S16	567231	8187014	3929	100	100	
85	P1-22	568256	8186391	3930	100	100	
86	S-PUC-20	568813	8185391	3919	100	100	Alluvial deposits (Thin layer)
87	P1-21	569757	8184397	3927	100	100	

Table 2, Continued

	ID	Easting (m)	Northing (m)	Surface Altitude SRTM (masl)	Tx (m)	Rx (m)	Investigated Formations
Profile 2							
88	P1-20	570437	8183297	3937	100	100	
89	P1-18	571497	8182989	3952	100	100	
	P1-17	572142	8182223	3957	100	100	Alluvial fan deposits (Minor alluvial fan)/Paleolacustrine deposits
90	P1-16	572365	8180766	3946	100	100	
91	P1-15	573208	8179750	3943	100	100	
92	S-LJ-02	573570	8178439	3932	100	100	
93	P1-14	574857	8177747	3939	100	100	
94	P1-13	575137	8176467	3929	100	100	
95	P1-12	575736	8175139	3922	100	100	
96	P1-11	576576	8174245	3925	100	100	
97	P1-10	576656	8173686	3923	100	100	
98	P1-9	577001	8173274	3925	25	25	
99	P1-8	577409	8172672	3924	100	100	
100	P1-7	577447	8172433	3923	100	100	Fluvioglacial/Paleolacustrine deposits
101	P1-6	577693	8172260	3924	100	100	
102	P1-5	578320	8172160	3933	100	100	
103	P1-4	578380	8171931	3933	100	100	
104	P1-3	578644	8171743	3934	100	100	
105	P1-2	578939	8171345	3931	100	100	
106	P1-1	579413	8170996	3936	100	100	
Profile 3							
	T-13	558610	8194231	3933.459754	100	100	
107	T12	557290	8193070	3909.535871	100	100	
108	S-PUC-12	555858	8191672	3880.6	100	100	
109	S-PUC-04	554545	8189869	3859.112097	100	100	Alluvial (Major alluvial fan)/Paleo-lacustrine deposits
110	S-PUC-11	553088	8188696	3851.8	100	100	
111	S-PUC-10	551617	8187506	3840.8	100	100	
112	S-PUC-09	550373	8186042	3838.5	100	100	
113	S17A	548678	8185697	3832	100	100	
114	S22A	546926	8185522	3831	100	100	
115	S18A	545412	8185735	3827	100	100	
116	S-PUC-14	543751	8185848	3826	100	100	Paleo-lacustrine deposits
117	T1	542396	8186425	3823.369384	100	100	
118	T2	541601	8187585	3828.299101	100	100	
119	T4	540372	8188270	3826.258777	100	100	
120	T5	539454	8189198	3824.454618	100	100	
121	T6	538579	8190210	3825.368	100	100	
	Profile 4						
122	S43E	536563	8182865	3826	100	100	
123	S43D	537202	8183360	3824	100	100	Paleo-lacustrine deposits
124	S43B	537682	8184071	3825	100	100	
125	S43A	538555	8184799	3826	100	100	

Table 2, Continued

	ID	Easting (m)	Northing (m)	Surface Altitude SRTM (masl)	Tx (m)	Rx (m)	Investigated Formations
126	**S44A**	539000	8185410	3826	100	100	
127	S45A	539618	8185927	3826	100	100	
128	T8	540205	8186431	3826	100	100	
129	T7	540750	8186936	3827	100	100	Paleo-lacustrine deposits
130	T2	541601	8187585	3828	100	100	
131	T3	541910	8187882	3826	100	100	
132	S39	542485	8188390	3826	100	100	
133	S40	542879	8189551	3828	100	100	
134	S41	542627	8190246	3839	100	100	
135	S42	542962	8190975	3863	100	100	Devonian Formation (Dbl)
136	S33	544451	8191530	3874	100	100	
Profile 4							
137	S34	544671	8192305	3834	100	100	
138	**S36**	545172	8193157	3825	100	100	Paleo-lacustrine deposits (Puerto Pérez bay 2)
139	S37	545348	8193806	3829	100	100	
140	S28	545468	8194296	3826	100	100	
141	S29	546048	8194788	3859	100	100	
142	S30	546661	8195431	3837	100	100	Tertiary Formations (Tcl, Tkk)
143	S31	546839	8195990	3844	100	100	
144	S32	546902	8196459	3850	100	100	
145	S32A	547239	8196936	3835	100	100	
146	S23	547959	8197459	3839	100	100	Paleo-lacustrine deposits (Puerto Pérez bay 1)
147	**S24**	548600	8198331	3838	100	100	
148	S24A	548495	8198865	3838	100	100	
149	S25	549100	8199117	3866	100	100	
150	S26	549969	8199364	3925	100	100	Devonian Formation (Dbl)
151	S26A	550563	8199673	3870	100	100	
Profile 5							
152	S62A	545446	8201362	3824	100	100	
153	S63	545811	8200792	3826	100	100	
154	S65	546029	8200404	3825	100	100	
155	S67	546123	8200060	3829	100	100	Paleo-lacustrine deposits
156	S69	546507	8199800	3827	100	100	
157	S-BT-07	547002	8199955	3829	100	100	
158	S-BT-08	547782	8198906	3833	100	100	
	S24	548600	8198331	3838	100	100	
Profile 6							
159	S56C	543187	8195247	3825	100	100	
160	S56B	543261	8195106	3823	100	100	
161	S56	543519	8194610	3826	100	100	
162	S58	543937	8194342	3825	100	100	Paleo-lacustrine deposits
163	S60	544249	8194091	3824	100	100	
164	S61	544535	8193631	3827	100	100	
	S36	545172	8193157	3825	100	100	

Table 2, Continued

	ID	Easting (m)	Northing (m)	Surface Altitude SRTM (masl)	Tx (m)	Rx (m)	Investigated Formations
Profile 7							
165	S48C	533688	8188494	3824	100	100	Paleo-lacustrine deposits
166	S48B	534247	8188382	3825	100	100	
167	S48	534923	8188411	3823	100	100	
168	S50	535488	8188024	3824	100	100	
169	S52	536172	8187698	3830	100	100	
170	S54	536673	8187527	3828	100	100	
171	T11	537011	8187048	3824.103133	100	100	
172	T10	537779	8186563	3827.660935	100	100	
173	T9	538426	8186018	3827.537339	100	100	
	S44A	539000	8185410	3826	100	100	
Other Soundings							
174	PC-1	583359	8165430	3929	25	25	Fluvioglacial deposits
175	PC-2	581907	8165700	3923	25	25	
176	PC-3	581232	8170281	3938	25	25	
177	SITE-1	576765	8153899	3861	100	100	Paleolacustrine deposits
178	SITE-2	588442	8188267	4464	100	100	Glacial deposits
179	SITE-3	577321	8153803	3863	100	100	Paleolacustrine deposits
180	SCH	547412	8193268	3835	100	100	Paleolacustrine deposits
181	S12B	564213	8187341	3916	100	100	Alluvial (Major alluvial fan)/Paleo-lacustrine deposits
182	T-16	563078	8185821	3896	100	100	
183	S12A	561646	8184526	3877	100	100	
184	S27	550889	8201358	3887	100	100	Devonian Formation (Dbl)
185	S19A	547143	8186039	3833	100	100	Paleolacustrine deposits
186	S21A	547156	8186379	3831	100	100	
187	S20A	547064	8186754	3833	100	100	

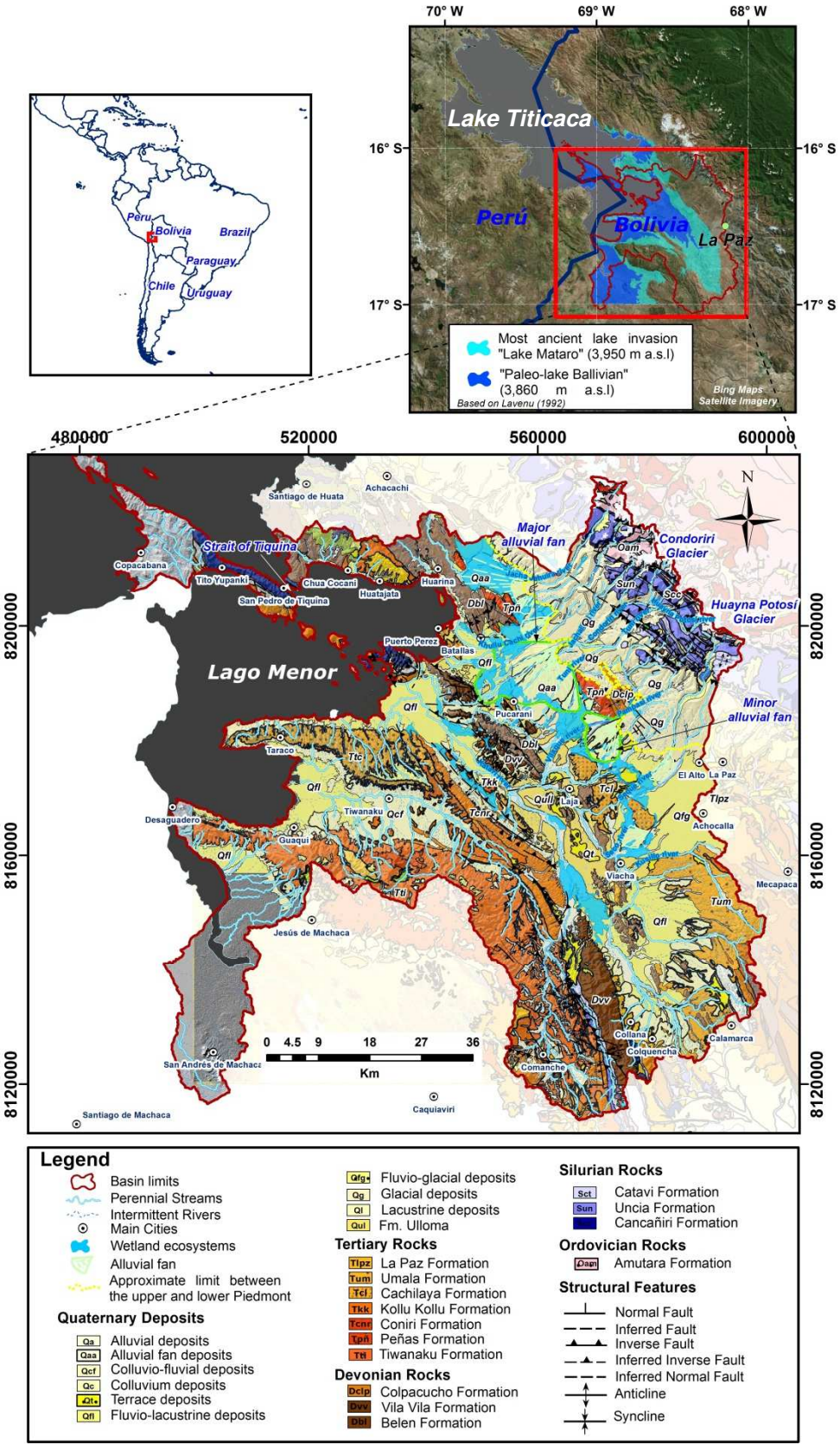

Figure 1. *(Top left) Location of the study area in South America. (Top right and Bottom) Study area showing the Katari and Lago Menor Basin, situated at the southeast of Lake Titicaca. It also shows the Geological and Morphostructural features of the basin (Based on geological data from G.E.O.S.I.R.H (2017) and GEOBOL & Swedish Geological AB (1995)).*

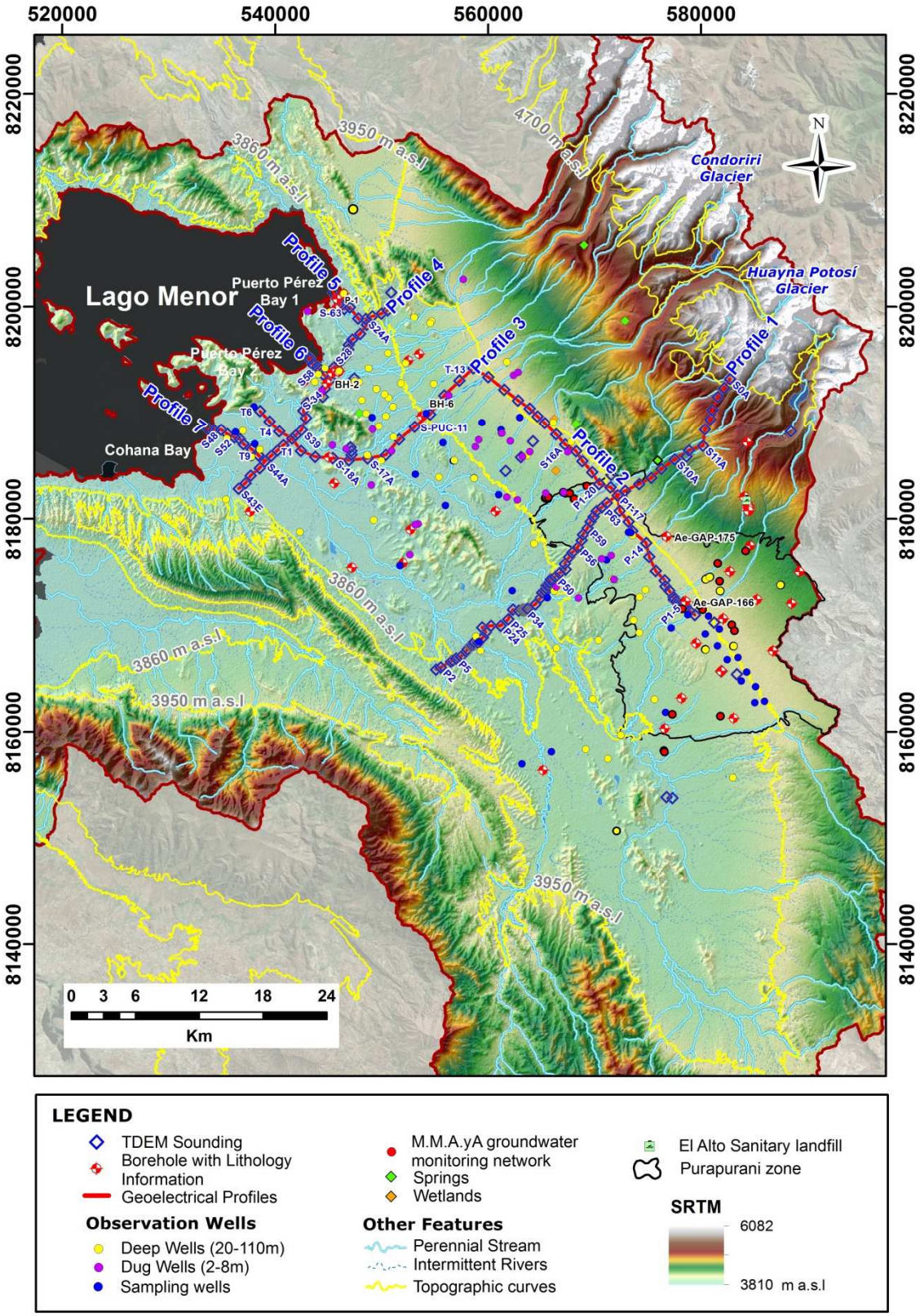

Figure 2. *Map of geophysical, groundwater level and geochemical measurements performed within the Katari and Lago Menor Basin. Hypsometric colours represent the elevation in meters above the sea level (m a.s.l) of the terrain (DEM: SRTM 1-Arc-Second Global-N.A.S.A, 2000).*